LIMNOLOGY
and
OCEANOGRAPHY: METHODS

ASLO

Limnol. Oceanogr.: Methods 2022

doi: 10.1002/lom3.10479

Toward bio-optical phenotyping of reef-forming corals using Light-Induced Fluorescence Transient-Fast Repetition Rate fluorometry

David J. Suggett,[1]* **Matthew R. Nitschke**,[1,2] **David J. Hughes**,[1] **Natasha Bartels**,[1] **Emma F. Camp**,[1] **Nicole Dilernia**,[1] **John Edmondson**,[3] **Sage Fitzgerald**,[1] **Amanda Grima**,[1] **Ayla Sage**,[4] **Mark E. Warner**[5]

[1]Climate Change Cluster, Faculty of Science, University of Technology Sydney, Ultimo, New South Wales, Australia
[2]School of Biological Sciences, Victoria University of Wellington, Wellington, New Zealand
[3]Wavelength Reef Cruises, Port Douglas, Queensland, Australia
[4]Rosenstiel School of Marine and Atmospheric Sciences, University of Miami, Miami, Florida
[5]College of Earth, Ocean, and Environment, University of Delaware, Lewes, Delaware

Abstract

Active chlorophyll *a* fluorometry is a well-established tool for noninvasively diagnosing coral functional state, but has not yet been developed as a rapid phenotyping (functional screening) platform as for agriculture and forestry. Here, we present a proof-of-concept using Light-Induced Fluorescence Transient-Fast Repetition Rate fluorometry (LIFT-FRRf) to identify coral photobiological-based phenotypes in the context of rapidly scaling coral propagation practices on the northern Great Barrier Reef. For example, resolving light niche plasticity to inform transplantation, and identifying functionally diverse colonies to maximize stock selection. We first used optically diverse laboratory-reared corals and coral endosymbiont (Symbiodiniaceae) isolates to develop a phenotyping approach integrating FRRf instantaneous kinetic parameters (light harvesting, electron turnover rates) and light-dependent parameters (dynamic "quenching" terms, saturating light intensity [E_K]). Subsequent field-based LIFT-FRRf phenotyping of coral from a selective (2-4 m depth) reef habitat revealed that widely topographically dispersed plating *Acropora* taxa exhibited broad light niche plasticity (E_K variance) underpinned by multiple phenotypes that were predominantly differentiated by minimum electron turnover capacity; fluorometer configurations that cannot resolve kinetic parameters will thus likely have more limited capacity to resolve phenotypes. As such, plating *Acropora* have broad propagation potential in terms of multiple functional variants for stock and across diverse light environments (growth, transplantation). In contrast, coral taxa (*Pocillopora verrucosa*, *Echinopora lamellosa*) with relatively restricted topographic dispersion exhibited less light niche plasticity and only single phenotypes, thereby imposing more constraints for propagation. We discuss the core technical, operational, and conceptual steps required to develop more sophisticated coral phenotyping platforms.

Coral reefs are degrading worldwide, with many stakeholders adopting "coral farming" propagation practices to maintain or rebuild local coral stocks (Boström-Einarsson et al. 2020) as part of locally targeted management toolkits. Such propagation of coral stocks is becoming increasingly industrialized as practices continue to scale, driving the desire for high-throughput biomarkers to guide the choice of corals that are grown (or outplanted) (Parkinson et al. 2019). Molecular-based markers of within-coral species genotypes and/or functional variants are in various stages of development and application (Baums et al. 2019; Morikawa and Palumbi 2019; Parkinson et al. 2019). In contrast, bio-optical-based markers remain relatively unexplored within coral reef restoration practices despite their well-developed applications into agriculture and forestry restoration (Yang et al. 2020). Active chlorophyll *a* (Chl *a*) fluorescence-based bio-optical methodologies and protocols to assess trait expression (i.e., "phenotyping," Yang et al. 2020)

*Correspondence: david.suggett@uts.edu.au

Author Contribution Statement: D.S., D.H., M.N., M.W. conceived the LIFT-FRRf concept, with A.S. and D.S. developing the recommendations. D.S., D.H., N.D., N.B. collected all laboratory data, and D.S., M.N., E.C., A.G., J.E. collected all field data, with S.F. leading the taxonomic separation methods for plating *Acropora* species. D.S., D.H., M.N. analyzed the data and led the manuscript writing, with all authors contributing to subsequent editorials in their specific areas of expertise.
Associate editor: Tammi Richardson

Additional Supporting Information may be found in the online version of this article.

have notably been established as new tools for crop management, with applications ranging from screening photosynthetic performance under altered gas availability in wheat (McAusland et al. 2019), to identifying barley with photochemical indicators of water–stress tolerance (Fernández-Calleja et al. 2020). Increasingly this bio-optical phenotyping is transitioning to smaller, cheaper fluorometers that can aid broad-scale high-throughput on-site surveying in real time (e.g., MultispeQ, Kuhlgert et al. 2016, Fernández-Calleja et al. 2020).

When applied to corals, active Chl *a* fluorometry rapidly and noninvasively assays photosystem II (PSII) photochemical activity of densely packed endosymbiotic dinoflagellates (Symbiodiniaceae) within the host tissues (Warner et al. 2010) but are also tailored to examine other endolithic or surface tissue-associated microalgae (Leggat et al. 2019). Decades of research on reef-forming corals and on cultured Symbiodiniaceae isolates have established that PSII activity varies with changing environmental factors that govern growth (Gorbunov et al. 2001; Suggett et al. 2015; Roberty et al. 2020) and stress susceptibility (Warner et al. 1999, 2006; Hoogenboom et al. 2012; Camp et al. 2019). In part, this variability reflects evolution of diverse modes of photosynthetic operation across Symbiodiniaceae species (or genotypes) (Roberty et al. 2014; Suggett et al. 2015; Wong et al. 2021) adapted to different environmental optima (Suggett et al. 2017), which in part may be driven by physical changes across host properties (e.g., tissue thickness; Wangpraseurt et al. 2019). Consequently, fluorescence-based parameters of PSII activity can be used to describe diverse functional types (i.e., phenotypes). Such phenotypes should inform how Symbiodiniaceae—and in turn their coral hosts—are photosynthetically adapted to long term environmental histories (e.g., low vs. high light types; Iglesias-Prieto et al. 2004, Suggett et al. 2015) as well as short-term environmental perturbations (e.g., heat stress; Goyen et al. 2017, Nitschke et al. 2018).

While Symbiodiniaceae photosynthetic performance certainly does not exclusively determine the extent of stress tolerance for reef-building corals (Cleves et al. 2020), how well corals process excitation (light) energy is a well-evidenced selecting agent towards growth and survival (reviewed by Warner and Suggett 2016) and therefore a significant factor underpinning ecological fitness. As such, the rapidly increasing pool of new fluorescence instruments and protocols for assaying PSII activity of corals (Szabó et al. 2017; Leggat et al. 2019; Gorbunov and Falkowski 2021)—including low-cost open-source variants (Hoadley and Warner 2017)—provides a logical framework to develop rapid phenotyping methods from active Chl *a* fluorescence that are already well established in terrestrial research and agriculture, but for targeted applications with corals.

We recently established the Great Barrier Reef's (GBR) first multispecies coral nursery and intensive mass out-planting practices (Suggett et al. 2020; Howlett et al. 2021) to aid maintenance and rehabilitation of "high-value" tourism reef sites. To date, selection of coral colonies—as well as "fragments of opportunity" (*see* Suggett et al. 2020)—has been at random from the neighboring reef site, adhering to permitting criteria of coral species population density and colony size. However, how well this random selection captures the inherent functional diversity for any given species remains unknown. Building on our recent use of basic active Chl *a* fluorescence parameters to resolve different Symbiodiniaceae phenotypes ("ecotypes," Suggett et al. 2015, Goyen et al. 2017), and of more sophisticated active fluorescence-based phenotyping of optically thick plants (Keller et al. 2019; Pleban et al. 2020), we therefore examined how Light-Induced Fluorescence Transient-Fast Repetition Rate fluorometry (LIFT-FRRf) (Kolber et al. 2005, 2019; Osmond et al. 2017, 2019) could identify coral with diverse functional performance in excitation energy processing. In doing so, we present a proof-of-concept for coral photo-physiological phenotyping, via multitrait descriptors of PSII light harvesting and utilization, that captures niche plasticity within and between coral taxa. We consider this proof-of-concept phenotyping in terms of the potential application to advancing coral propagation practices; specifically, using LIFT-FRRf to capture the extent with which (i) local coral species are functionally diverse (exhibit different photo-physiological phenotypes), needed to ensure targeted stock choice for coral propagation maximizes diversity and hence resilience (*sensu* Baums et al. 2019), and (ii) different phenotypes are "physiologically plastic" (photo-physiological dynamic range) and hence define the extent that any given phenotype can be successfully moved across diverse reef environments. How the different photo-physiological phenotypes ultimately captured are indicative of growth and survivorship—key success metrics used in coral restoration (Suggett et al. 2020)—is the subject of future work.

Materials and procedures

LIFT-FRRf coral phenotype concept

LIFT-FRRf describes specific models of FRR fluorometer developed for remote monitoring of terrestrial plant photosynthetic performance (Kolber et al. 2005, 2019; Osmond et al. 2017, 2019) and, as we employ here, also for direct probing of liquid (microalgal culture, seawater, etc.; Levin et al. 2017) or small coral biopsy samples (Szabó et al. 2017) retained within an internal optical chamber. While FRRf (Leggat et al. 2019) and other approaches (e.g., Fluorescence Induction and Relaxation fluorometry; Hennige et al. 2011) have been used to assay coral photo-physiology—including submersible versions (Gorbunov et al. 2001; Levy et al. 2003)—an alternate approach, pulse amplitude modulation (PAM) fluorometry has largely been applied to study coral to date (*see* also Warner et al. 2010). PAM fluorometry is programmed to deliver a modulating light and periodic prolonged saturating

flash to determine the minimum and maximum fluorescence ("amplitude-based" protocol). In contrast, FRRf protocols employ a series of sub-saturating flashlets to also determine the minimum and maximum fluorescence, but in doing so captures the dynamic kinetics underlying maximum fluorescence saturation and subsequent decay (Kolber et al. 1998, 2005). This alternate "kinetics-based" protocol therefore enables much deeper parameterization of photo-physiological functioning than purely amplitude-based protocols, and we refer the reader to recent reviews on the broad and fundamental principles of these and other active Chl *a* fluorescence bio-optical measurements (Hughes et al. 2018; Schuback et al. 2021). Another important feature of PAM-type protocols is that the maximum fluorescence yields obtained from the prolonged saturating pulse are perturbed according to the redox state of the plastoquinone (PQ) pool (oxidized PQ is a quencher of fluorescence whereas its reduced form—plastoquinol—is not) (*see* Suggett et al. 2003, 2010 and references therein). As such, accurate retrieval of photo-physiological parameters derived from the primary amplitude-based measurements is confounded where extrinsic environmental and/or intrinsic biological factors simultaneously regulate PQ pool redox state—as we have previously demonstrated in side-by-side comparisons of PAM and FRR fluorometers (Suggett et al. 2003, 2010). Therefore, while PAM or indeed any form of active Chl *a* fluorometer could conceivably be used to develop phenotyping platforms, we use LIFT-FRRf to maximize accurate parameter retrieval as a logical starting point for our proof-of-concept with coral.

LIFT-FRR fluorometers are equipped with multiple excitation wavelengths; however, we restricted our proof-of-concept here to a single excitation protocol (combining two peak λ values, 445 and 505 nm) to optimize absorption by coral endosymbionts (Szabó et al. 2014; Wangpraseurt et al. 2014; Leggat et al. 2019). LIFT-FRRf specifically employs a series of short flashlets to manipulate saturation-relaxation of the primary quinone acceptor of the PSII reaction center (RCII), Q_A (Z. Kolber pers. comm.; Kolber et al. 1998, 2005, Osmond et al. 2017, 2019) (Fig. 1). An initial saturation protocol cumulatively reduces Q_A—and so increasingly "closes" the RCII pool—to yield a transient rise in fluorescence from minimum to maximum (F_0 to F_m, F' to F_m'; in darkness, under actinic light, respectively) (*see* Table 1 for terms and definitions). This rise is governed by the PSII effective absorption cross section (σ_{PSII}, σ_{PSII}'), which itself is regulated by the physical arrangement and type of pigments for light harvesting, as well as the nature of RCII "connectivity" (ρ, ρ') (Kolber et al. 1998; Suggett et al. 2004; Oxborough et al. 2012). Multiplying σ_{PSII} by the number of functional RCIIs (n), and normalized to the maximum PSII photochemical efficiency ($F_v/F_m = [F_m - F_0]/F_m$) to account for nonradiative loss terms inherent to σ_{PSII}, yields the absorption coefficient for the PSII light harvesting complex, termed a_{LHCII} ($= [\sigma_{PSII} \cdot n] \cdot [F_v/F_m]^{-1}$) (Kolber et al. 1998; Oxborough et al. 2012; Suggett et al. 2015). In corals, values for σ_{PSII} as well as maximum and minimum fluorescence (but not F_v/F_m)—and hence a_{LHCII}—are influenced by polyp expansion (Levy et al. 2003) via alterations to optical properties of the tissues (Wangpraseurt et al. 2019).

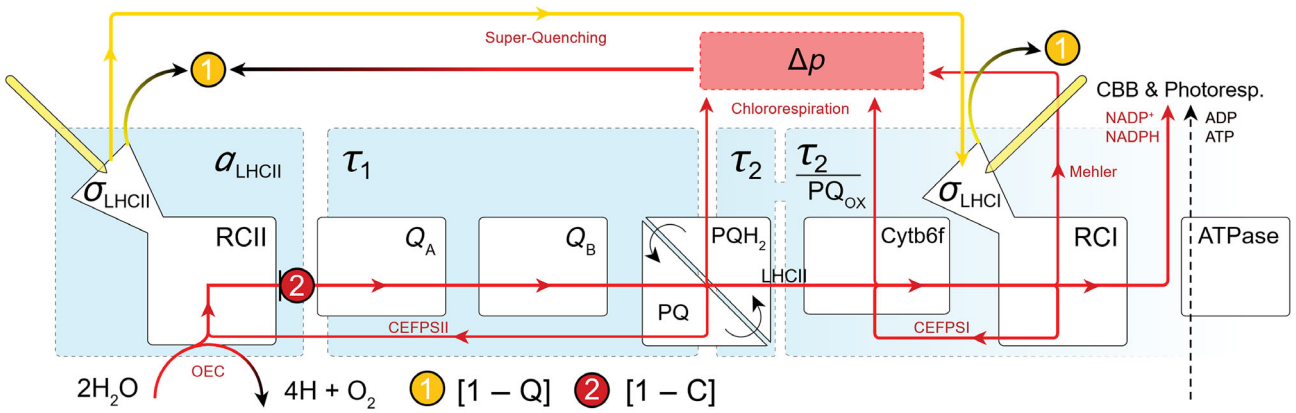

Fig. 1. Schematic representation of PSII photochemical operation and relationship to parameters retrieved using LIFT-FRRf (modified from Hughes et al. 2018). Specifically, light is absorbed through PSII light harvesting antennae (σ_{PSII}) coupled to PSII reaction centers ([RCII]) of the oxygen evolving complex (OEC); noting that strictly, only functional RCIIs (*n*, *see* Table 1) support oxygen evolving capability at any given time. Normalizing σ_{PSII} to the maximum PSII photochemical efficiency (F_v/F_m) yields the effective cross section of light harvesting complex II (σ_{LHCII}) and accounting for *n* yields the absorption coefficient for PSII (a_{LHCII}). The proportion of all [RCII] "engaged" (passing electrons downstream) yields the extent of photochemical "quenching" ([1 – *C*]). Electrons are passed downstream via a series of electron carriers (Q_A, Q_B, PQ pool, cyt b_6f) to PSI, which are described by a series of turnover time constants (τ_1, τ_2, τ_2/PQ_{OX}). Together, electron transfer through PSII and PSI drives the generation of energy (ATP) and reductant (NADPH) used—in part—for CO_2 uptake through the Calvin Benson-Bassham (CBB) cycle. A proportion of excitation energy is further dissipated by dynamic nonphotochemical (heat) dissipation pathways (the extent of which is defined here as [1 – Q]) that are activated and build through excitation pressure (in part via proton motive force, Δp). Photochemical and/or nonphotochemical electron turnover is further modified by additional electron (energetic) sinks (e.g., cyclic flow around PSII and PSII; CEFPSII, CEF, PSI; Mehler) to optimize excitation pressure.

A subsequent relaxation protocol cumulatively reoxidizes Q_A governed by several time constants for electron transfer (τ) to subsequent electron carriers; for example, Osmond et al. (2017, 2019) (also Kolber et al. 1998; Szabó et al. 2017), describe two time constants, τ_1 and τ_2, to represent maximum electron transfer capacity from Q_A to PQ and for PQ pool reoxidation, respectively. A third time constant describing the maximum downstream transfer of electrons from PQ to photosystem I (PSI) can be further retrieved by normalizing τ_2 by the oxidized portion of the PQ pool (PQ_{OX}). Parameterization of PQ_{OX} is retrieved from a model describing electron turnover from Q_A to PQ, size of the PQ pool, capacity of the PQ pool in electron equivalents, and PQ pool reoxidation (Z. Kolber pers. comm.), and where the size of the PQ pool ranges from 5 to 12 quinones per reaction center (Suslichenko and Tikhonov 2019, and references therein). Descriptions and evaluation of the various models behind the kinetic parameter retrieval is presented elsewhere (Kolber et al. 1998, 2005, Osmond et al. 2017, 2019; https://soliense.com/LIFT_Method.php, accessed 21st December 2021). Together, a_{LHCII} describes light harvesting capacity while the turnover time constants describe subsequent light utilization capacity, whereby τ_1, τ_2, and τ_2/PQ_{OX} monitor the PQ pool control loop that underpins maximum electron transfer rates (Osmond et al. 2019; Gorbunov and Falkowski 2021).

Interplay between a_{LHCII} and time constants for electron transfer determines where photochemistry transitions from light dependence to light independence, otherwise termed E_K (Hughes et al. 2018; Nitschke et al. 2018). E_K values retrieved from active fluorescence are often variable across coral species (Kaniewska et al. 2014), as well as photo-acclimation history based on light availability from season and depth (Hennige et al. 2008; Suggett et al. 2012; Nitschke et al. 2018). Hence, E_K variance for any given coral taxa therefore reflects the ecological niche width achievable through photo-acclimation to the prevailing light history, but whether this is the result of one or more phenotypes—through differential modification of kinetic parameters a_{LHCII} vs. τ—remains unexplored.

Photobiological descriptions of a_{LHCII} and τ—often from dark- or low-light acclimated samples—provide key insight of the maximum potential for light harvesting and utilization. However, "instantaneous" measurements under transient conditions, such as the continuously dynamic light environments for benthic corals (Anthony et al. 2004), are needed to capture the realized responses underpinning functional performance (Hughes et al. 2018; Gorbunov and Falkowski 2021). Numerous factors operate to "downregulate" (in efforts to maintain optimum) PSII photochemistry in coral endosymbionts (Vega de Luna et al. 2020; reviewed by Warner and Suggett 2016); as such, parameterizing light harvesting and utilization in the light (i.e., σ_{PSII}', τ_1', etc.) provide additional descriptors of the photochemical operation dynamics (Gorbunov et al. 2001; Szabó et al. 2017). However, accurately resolving these kinetic parameters becomes increasingly more challenging (and potentially more inaccurate) as dynamic light exposure increases and variable fluorescence correspondingly decreases (Hughes et al. 2018; *see* Gorbunov and Falkowski 2021). To overcome this constraint, active fluorescence induction signatures are typically parameterized to capture dynamic trade-offs among photochemistry and "downregulation" via "quenching" terms calculated from minimum and maximum fluorescence; for example, we have shown that under the same conditions, coral endosymbionts as free living cultures (Suggett et al. 2015) or in hospite (Nitschke et al. 2018) employ different photosynthetic strategies based on trade-offs in photochemical vs. nonphotochemical quenching (derived as $[1 - C]$ and $[1 - Q]$, respectively; *see* "Materials and procedures" section) reflecting different cellular machinery available for dissipating excitation energy (Hughes et al. 2018; Vega de Luna et al. 2020). We acknowledge that additional photobiological parameters could ultimately be applied for phenotyping (Kuhlgert et al. 2016; Yao et al. 2018; Keller et al. 2019; McAusland et al. 2019; Pleban et al. 2020), but how dynamic quenching factors compliment a_{LHCII} and the turnover time constants (Fig. 1) provides a logical framework to initially explore proof-of-concept coral photo-physiological phenotyping given that these parameters have each been independently examined through prior active fluorometry studies in corals.

Laboratory sampling

Aquarium-maintained corals (orders: Scleractinia and Alcyonacea) as well as endosymbiont isolates (family: Symbiodiniaceae) held within a long-term culture collection at the University of Technology Sydney were initially used to explore and optimize LIFT-FRRf data collection. Within the aquarium system, 16 coral species (including colonies of different color morphs for *Pocillopora damicornis*, and 2 different colonies for each of *Fungia* sp. and *Acropora tenuis*; total $n = 19$ colonies, *see* Supporting Information Table S1)—all originally sourced from the GBR (*Majestic Aquariums*, Taren Point, NSW, Australia)—were maintained under reef growth conditions as detailed in Supporting Information Methods S1. We selected eight algal isolates representing multiple Symbiodiniaceae genera (Supporting Information Table S1; also Ros et al. 2020) with known differences in photosynthetic function to light intensity (Suggett et al. 2015; Ros et al. 2020) and/or heat stress (Goyen et al. 2017). Algal isolates were maintained in F/2 media in exponential growth—via regular cell counts and dilutions (Suggett et al. 2015)—under 25°C and a downwelling irradiance of 85 ± 15 μmol photons m^{-2} s^{-1} (Philips TLD 18 W/54 fluorescent tubes, 10,000 K on a 12 h : 12 h light: dark cycle).

Field sampling

To further assess the range in phenotypic signatures in corals, several species were collected at Opal Reef, on the northern GBR (16°13′S 145°53.5′; 24.7 km^2), at sites "RayBan,"

"Blue Lagoon," and "Mojo," where coral nurseries and out-planting have been underway since 2018 (Howlett et al. 2021). As with other reef sites of the GBR, plating (tabular) Acroporid corals at Opal Reef were particularly impacted by the 2016/2017 back-to-back mass coral bleaching events (Hoogenboom et al. 2017; Hughes et al. 2017), and so represent priority species for nursery-based site rehabilitation (e.g., *Acropora* cf. *hyacinthus*; Howlett et al. 2021), and therefore the focus to examine for intraspecies phenotypes. Sites of Opal Reef that were less impacted by recent heat waves are characterized by many plating colonies of *Acropora* across all topographies, with other taxa more topographically restricted (e.g., *Echinopora lamellosa* and *Pocillopora verrucosa*, which predominantly grow on cryptic or exposed reef topography, respectively) (John Edmondson, David Suggett, Emma Camp pers. obs.). We therefore sampled across colonies of plating Acroporids, *E. lamellosa* and *P. verrucosa*, to test the hypothesis that the latter two more topographically restricted taxa would exhibit relatively conserved intraspecies phenotypes compared to the more topographic diversely distributed plating Acroporid taxa.

Coral fragments were collected by SCUBA (4–7 February 2020) from colonies between 2 and 4 m depth. Each colony was photographed to verify species identity (detailed below), and a 3- to 5-cm-length branch fragment removed from the plate growing edge with bone cutters. Fragments were returned to the operations vessel (*Wavelength* 5) and held in aerated tanks filled with reef water until measured with LIFT-FRRf (within 1–2 h of sampling). Plating Acroporid species were identified as *A. hyacinthus* and *Acropora. cytherea*, which are part of known species complexes with up to four *A. hyacinthus* and two (*A. cytherea*) molecular distinct species that occur on the GBR (Ladner and Palumbi 2012). For the purpose of this study, samples were categorized into potential morpho-species, where only three and two distinctive species were found for *A. hyacinthus* and *A. cytherea*, respectively. *A. hyacinthus* sp-1 (i.e., notional *A.* "*hyacinthus*" species 1), sp-2, and sp-3 all have vertical branchlets with labellate flaring lip (sometimes rounded lip) radials that form rosettes around the axial tip. Distinctive features to delineate these morpho-species are (i) uneven and indeterminate growth and spacing of vertical branchlets with slightly exert axial tips (*A. hyacinthus* sp-1); (ii) pastel-like colony coloring, distinctly compact and uniform growth and spacing of vertical branchlets with no exert axial tip (*A. hyacinthus* sp-2); and (iii) thicker branchlets compared to other morpho-species, has a fused colony center, and branchlets grow angular, fanning out toward growth edge tips (*A. hyacinthus* sp-3). *A. cytherea* all have long thin vertical branchlets, multiple layered growth edge tips and small radials (compared to axials) with vertical growth directions of radial lips. Distinctive features to delineate these morpho-species are: (i) multiple messy incipient axials growing off branchlets, rounded lip radials and slightly exert axial tip (*A. cytherea* sp-1); and (ii) neat thin branchlets with long pointed lip radials that can grow past the axial tip, and an often-deformed axial opening (*A. cytherea* sp-2). Example photographs are given in Supporting Information Fig. S1. Over the four sampling days, a total of 24, 4, 4, 9, and 3 colonies of *A. hyacinthus* sp-1 (Ah-1), *A. hyacinthus* sp-2 (Ah-2), *A. hyacinthus* sp-3 (Ah-3), *A. cytherea* sp-1 (Ac-1), and *A. cytherea* sp-2 (Ac-2), respectively, were sampled and analyzed with LIFT-FRRf.

Light-induced fluorescence transient-fast repetition rate fluorometry

All fragments or algal cultures were low light (ca. 5–10 μmol photons m^{-2} s^{-1}) acclimated for at least 30 min prior to LIFT-FRRf (Soliense Inc., USA) measurements. Such acclimation under low light is favored over complete darkness to ensure any dynamic nonphotochemical quenching is relaxed without inducing chlororespiration, which can modify the redox state of PQ pool (Suggett et al. 2015, and references therein). All LIFT-FRRf programming and model fitting was conducted using a custom-designed application software package (https://soliense.com/LIFT_Method.php, accessed 21 December 2021; Z. Kolber pers. comm.; *see* also Osmond et al. 2017, 2019) that describes the relationship between the excitation, fluorescence, and PSII photosynthetic properties (Kolber et al. 1998). At the time of measurement, either (i) a biopsy of tissue and skeleton of ca. 1–2 mm^2—often as a full or partial corallite—was gently removed from each coral fragment with scalpel and forceps (ca. 1–2 cm below the branch tip, always surface side up and avoiding the axial/terminal polyp) to ensure the biopsy remained intact, and the sample placed in the LIFT-FRRf optical chamber filled with filtered seawater passed through 0.2-μm syringe filters (Minisart NML, Sartorious, Göttingen, Germany). Biopsies were visually inspected and discarded if not intact and a new biopsy taken; or (ii) aliquots of ca. 2 mL Symbiodiniaceae culture were used to fill the LIFT-FRRf optical chamber. The LIFT-FRRf was programmed to deliver single turnover (ST) fluorescence transients consisting of 100 flashlets of 1.6 μs at 2.5 μs intervals for Q_A reduction, followed by 127 flashlets of 1.6 μs at exponentially increasing intervals over $\sim$ 30 ms for Q_A reoxidation. ST excitation was provided by both the 445- and 505-nm LEDs, and hence all values of σ_{PSII} reported here are inherently weighted to this combination of wavelengths (*see* Suggett et al. 2004). Each fluorescence transient was corrected for baseline fluorescence, which consisted of filtrate of reef/aquaria seawater or algal culture gently passed through a 0.2-μm syringe filter (Minsart NML, Sartorious) and acquisitions recorded iteratively from 10 consecutive fluorescence transients. Each acquisition was then fit against the photophysiological model of Kolber et al. (1998), with fitting functions of ρ (connectivity) and quenching of triplet P680 set to 0.2 and "off," respectively, and a double exponential decay for electron turnover through sequential electron carriers.

Acquisitions were made continuously during two alternate protocols. For the routine phenotyping assays, we employed a rapid fluorescence light curve (FLC) protocol following an

Table 1. Photo-physiological parameters and derivations (where applicable) used here with LIFT-FRRf, and whether they are sourced by amplitude-based (A) or kinetic-based (K) protocols. Bold text indicates LIFT-FRRf parameters utilized to identify coral phenotypes. Units for amplitude-based parameters are instrument specific for primary fluorescence parameters and dimensionless for secondarily derived parameters (factors or ratios using the primary fluorescence parameters). All kinetic parameters are derived from models fit to LIFT-FRRf induction and relaxation acquisitions (and units shown alongside the respective definition); these various models are described and evaluated elsewhere (Kolber et al. 1998, 2005, Osmond et al. 2017, 2019; https://soliense.com/LIFT_Method.php, accessed 21 December 2021).

Parameter	Definition	Source	Derivation
[1 − *C*]	Photochemical energy dissipation	A	$[F_m' - F']/[F_m' - F_0']$
[1 − *Q*]	Dynamic nonphotochemical energy dissipation	A	$([F_m' - F_0']/F_m')/(F_v/F_m)$
$\boldsymbol{a_{LHCII}}$	Absorption coefficient for the PSII light-harvesting complex (Å^2)		$[\sigma_{PSII} \cdot n] \cdot [F_v/F_m]^{-1}$
$\boldsymbol{E_K}$	Saturating light intensity	—*	
F'	Fluorescence yield under actinic light at time t	A	
F_0	Minimum PSII fluorescence (dark-regulated state)	A	
F_0'	Minimum PSII fluorescence (light-regulated state)	A	$F_0/([F_v/F_m] + [F_0/F_m'])$
F_m, F_m'	Maximum PSII fluorescence (dark-, light-regulated state)	A	
F_v, F_v'	Maximum variable PSII fluorescence (dark-, light-regulated state)	A	$F_m - F_0$, $F_m' - F_0'$
$\boldsymbol{F_v/F_m}$	Maximum photochemical efficiency (dark-regulated state)	A	$[F_m - F_0]/F_m$
F_v'/F_m'	Maximum photochemical efficiency (light-regulated state)	A	$[F_m' - F_0']/F_m'$
F_q'/F_m'	Effective photochemical efficiency (light-regulated state)	A	$[F_m' - F']/F_m'$
σ_{PSII}, σ_{PSII}'	Effective absorption cross-section of PSII (dark-, light-regulated state) (Å^2 quanta^{-1})	K	
$\boldsymbol{\sigma_{LHCII}}$	Effective cross-section of PSII light harvesting (dark-, light-regulated state) (Å^2 quanta^{-1})		$\sigma_{PSII}/(F_v/F_m)$
σ_{LHCII}'	Effective cross-section of PSII light harvesting (light-regulated state) (Å^2 quanta^{-1})		$\sigma_{PSII}'/(F_v'/F_m')$
[RCII]	PSII reaction center abundance	—†	
n	Functional [RCII]	—†	
ρ, ρ'	PSII connectivity factor (dark-, light-regulated state)	K	
$\boldsymbol{\tau_1}$	Minimum electron turnover time (Q_A to PQ) (μs)	K	
$\boldsymbol{\tau_2}$	Minimum electron turnover time for PQ pool reoxidation (μs)	K	
PQ_{OX}	Oxidized portion of the PQ pool	K	
$\boldsymbol{\tau_2/PQ_{ox}}$	Transfer time for electrons from PQ pool to photosystem I (μs)	K	

*Derived from Eq. 4 (fit to the light response of F_q'/F_m'; main text).
†The reaction center abundance that must be sourced based on independent measurements using biochemical approaches, which has units according to the user-preferred normalization (e.g., RCII per sample volume, per chlorophyll content or per cell), *see* the main text; Oxborough et al. 2012).

initial dark step. The light protocol was delivered by only the 445-nm LED (0, 10, 25, 50, 100, 150, 250, 500, 750, 1000, and 1250 μmol photons m^{-2} s^{-1}), with each light step lasting 30 s and collection of three acquisitions. A separate subsample for the laboratory experiments was subjected to a second "quenching protocol" consisting of an initial dark step followed by 1200 s under 500 μmol photons m^{-2} s^{-1} (also 445 nm) for comparing how dynamic fluorescence parameters retrieved from short-term light exposure—and hence the FLC—compared to those retrieved under longer-term light exposure. All light-response protocols were used to retrieve (i) initial dark-acclimated maximum light harvesting and turnover potential (kinetic parameters a_{LHCII}, τ_1, τ_2, τ_2/PQ_{OX}) and further parameterize (ii) light-activated phenotype characteristics for dynamic energy quenching (derived from amplitude measurements of maximum and minimum fluorescence). Determination of a_{LHCII} requires input of σ_{PSII}, F_v/F_m and n, where n is based on variations in F_0/σ_{PSII} weighted against an instrument-specific calibration of functional RCII abundance (Oxborough et al. 2012; Boatman et al. 2019), where n can be normalized per volume of sample, per Chl *a* concentration or per cell, as required (Table 1). Since the LIFT-FRRf has not been calibrated with independent measurements of PSII reaction center abundance (Oxborough et al. 2012), we simply treated light absorption as the term σ_{LHCII} (PSII effective cross section normalized to maximum quantum yield [$=\sigma_{PSII}/(F_v/F_m)$]; Oxborough et al. 2012, Suggett et al. 2015).

Photochemical ([1 − *C*]) and dynamic nonphotochemical (downregulated, [1 − *Q*]) energy dissipation was determined as per Suggett et al. (2015),

$$[1-C] = [F_m' - F']/[F_m' - F_0'], \quad (1)$$

$$[1-Q] = ([F_m' - F_0']/F_m')/(F_v/F_m), \quad (2)$$

$$F_0' = F_0/[(F_v/F_m) + (F_0/F_m')]. \quad (3)$$

We use the term $[1 - Q]$ to describe dynamic nonphotochemical quenching (as opposed to other popularly used—but unbounded—terms such as NPQ = $[F_m - F_m']/F_m'$) since, as with $[1 - C]$, values for $[1 - Q]$ are bounded between values of 0 and 1, and where the PSII photochemical efficiency ($[F_m' - F']/F_m'$, termed F_q'/F_m') equals the product of [1 − C] and ($[1 - Q] \cdot F_v/F_m$) and thus a convenient means to examine for trade-offs in quenching strategy governing photochemistry (Suggett et al. 2015). Importantly, $[1 - Q]$ is derived from the term "Q_m" (excitation pressure over PSII) (Iglesias-Prieto et al. 2004; see Suggett et al. 2015), where Q_m increases with nonphotochemical quenching (and so $[1 - Q]$ decreases). Similarly, values of $[1 - C]$ decrease as the proportion of RCIIs engaged in photochemistry increases. For the phenotyping, we specifically only used values of $[1 - C]$ and $[1 - Q]$ generated from the highest (final) light intensity of the FLC (FLC-1250 μmol) so as to capture the greatest dynamic quenching via the rapid FLC assay.

As part of our analysis, we also determined the saturating light intensity (E_K) for photochemistry from the FLC, which is again weighted to the actinic light wavelength (445 nm), as per Nitschke et al. (2018). E_K was retrieved for each FLC using the following model that describes the light (E) dependency of PSII photochemistry (Hennige et al. 2008):

$$F_q'/F_m' = \left[\left(F_q'/F_m'(\max) \cdot E_K\right) \cdot (1 - \exp(-E/E_K))\right]/E. \quad (4)$$

Fitting was performed in R using the nls_multstart (Padfield et al. 2016) R package which employs the *nlsLM* function in the minpack.lm (Elzhov et al. 2013) R package. Briefly, model selection was carried out using the Akaike information criterion (AIC) to identify the value of E_K, which best characterized each FLC. This entailed running 250 different random combinations of starting parameters drawn from a uniform distribution of hypothetical, predefined minimum and maximum values (5 and 1250 μmol photons m^{-2} s^{-1}, respectively), and retaining the parameter set that returned the lowest AIC score.

Data analysis

Each parameter (σ_{LHCII}, τ_1, τ_2, τ_2/PQ_{OX}, $[1 - Q]$, and $[1 - C]$) was assessed for normality using the bestNormalize R package (Peterson and Cavanaugh 2020), which evaluates the normalization efficacy of many candidate transformations, of which the best is selected using the Pearson P statistic. Improvements to normality were also assessed manually through visualization of a QQ-plot. Normalized data were zero-mean standardized using the *decostand* function in the R package vegan (Oksanen et al. 2015). Nonmetric multidimensional scaling (NMDS) was employed by calculating a Euclidean distance matrix and ordination using the *metaMDS* function in vegan. The *envfit* function in vegan was used to examine the ordination–parameter relationships by correlating the sample ordination space with the normalized-standardized parameter data, producing vectors that indicate the projection of maximum correlation. Significance of individual parameters was assessed through 999 permutations against an alpha value of 0.05. Sample clustering that is indicative of distinct phenotypes was examined by using the "average" agglomeration method from the NBClust R package (Charrad et al. 2014) that applied to the Euclidian distance matrix, and the optimal number of clusters determined by querying all indices, specifying the min/max number of clusters at 2 and 7, respectively. Results of the NMDS ordination, *envfit* vectors, and clustering, were visualized using ggplot2 (Wickham 2016).

Assessment

Laboratory coral and endosymbiont signatures

Extent of dynamic quenching captured is a direct consequence of the actinic protocol, in terms of light intensity and duration (Suggett et al. 2003, 2015; Osmond et al. 2017). We therefore first examined whether and how values for $[1 - C]$ and $[1 - Q]$ from the highest light intensity of the FLCs (FLC-1250 μmol) (Fig. 2A,B) compared with those generated under relatively short (360 s) vs. long (1200 s) exposure to constant saturating light (500 μmol photons m^{-2} s^{-1}) (CONST-500 μmol) across our diverse range of aquarium corals and Symbiodiniaceae culture isolates. A striking feature of the constant light exposure treatment was initiation of extreme nonsteady-state fluorescence perturbations upon transition from dark to "lights on" (here, 500 μmol photons m^{-2} s^{-1}). Specifically, initial inductions of $[1 - C] < 0$ (and $[1 - Q] > 1$) that subsequently settle to higher (and lower) steady-state values under continued light exposure (Fig. 2C,D). Such dynamics reflect transition between light steps and nonsteady-state quenching (and fluorescence yields) where photochemical pathways reequilibrate to the new light dose, processes that are most pronounced for greater shifts of consecutive light intensities (Suggett et al. 2003). The examples in Fig. 2A–D for the corals *Turbinaria peltata* and *Oulophyllia* sp. demonstrate that these nonsteady-state transients were consistently evident despite very different quenching dynamics; notably, *T. peltata* exhibited slower and smaller declines in $[1 - Q]$ (and slower but greater increases in $[1 - C]$), and thus relatively slow induction of nonphotochemical quenching to gradually relieve excitation pressure from RCII turnover, over time under constant light exposure. In contrast, *Oulophyllia* sp. largely retained the same $[1 - C]$ alongside rapid and relatively high reduction in $[1 - Q]$ over time (and where $[1 - Q]$ does not fully recover to preexposure levels when lights are turned off), suggesting fast and sustained generation of "locked in" downregulation that relieved relatively little RCII turnover.

Despite presence of inherently different quenching dynamics, values of $[1 - C]$ for FLC-1250 μmol from across all coral and Symbiodiniaceae samples in fact closely correlated with those for CONST-500 μmol after both 360 and 1200 s exposure ($r^2 > 0.89$), with values of $[1 - C]$ consistently higher—

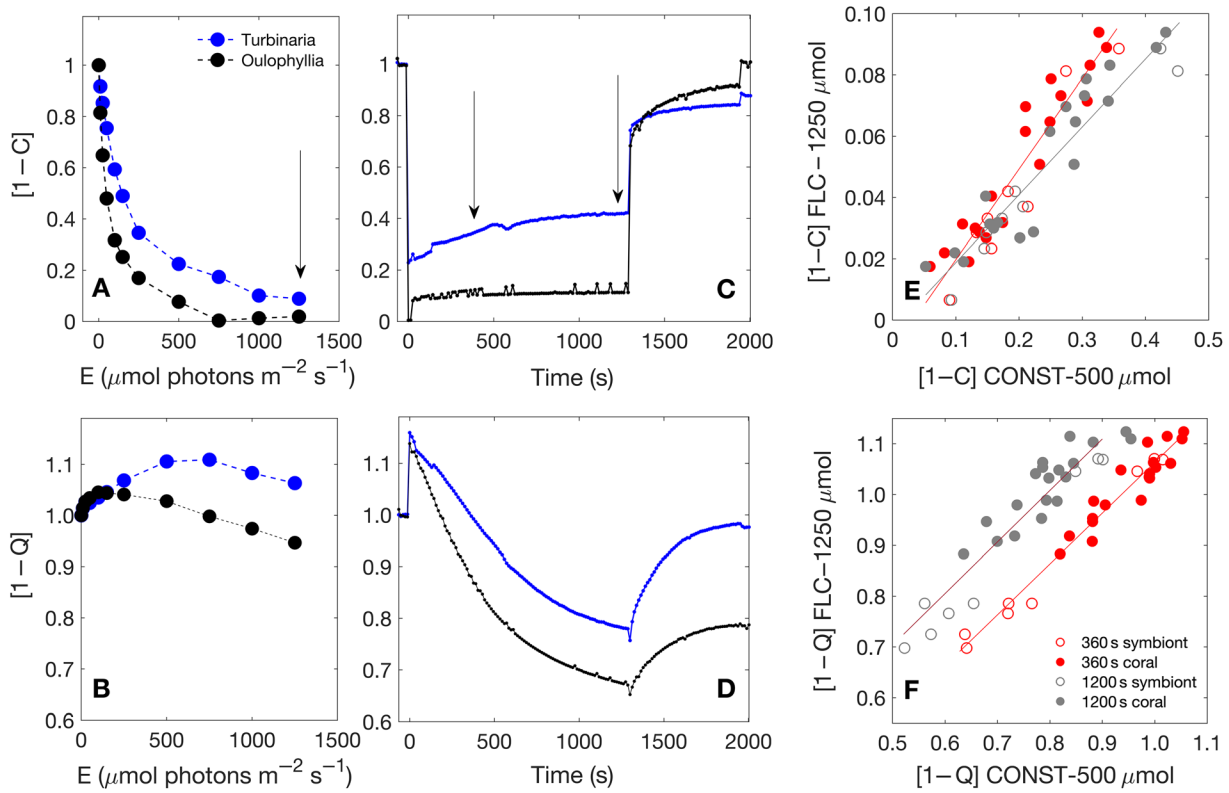

Fig. 2. LIFT-FRRf-derived photochemical and nonphotochemical ([1 − *C*] and [1 − *Q*] respectively, dimensionless; Eqs. 2 and 3) quenching dynamics. Panels (**A**–**D**) are shown as contrasting quenching dynamics retrieved from two examples of aquarium-maintained coral species, *Turbinaria peltata* and *Oulophyllia* sp. Panels (**A**,**B**) are the rapid FLCs conducted via increasing light intensity (**E**, μmol photons m^{-2} s^{-1}) every ~ 30 s. The arrow indicates data under 1250 μmol photons m^{-2} s^{-1} (= FLC-1250 μmol). Panels (**C**, **D**) are the constant "quenching protocol" consisting of an initial dark step followed by ~1300 s under 500 μmol photons m^{-2} s^{-1}, and then a "recovery" period under ~ 700 s of 5 μmol photons m^{-2} s^{-1} and finally 30 s darkness. The arrows indicate data under 360 and 1200 s of constant light (= CONST-500 μmol). Actinic irradiance used across all protocols **(A-D)** was delivered via 445-nm LEDs (*see* the main text). Panels (**E**, **F**) are quenching values extracted from all coral species samples (n = 19): Symbiodiniaceae isolates (n = 8) species are examined; specifically **(E)** [1 − *C*] FLC-1250 μmol vs. [1 − *C*] CONST-500 μmol and **(F)** [1 − *Q*] FLC-1250 μmol vs. [1 − *Q*] CONST-500 μmol, and red vs. gray circles represent data for CONST-500 μmol collected after 360 s vs. 1200 s, respectively. Regression slopes are shown in panels (**E**,**F**) with correlation coefficients and regression equations given in Supporting Information Table S2.

and hence with fewer RCIIs engaged in photochemistry at any one time—after 1200 s compared to 360 s (Fig. 2E; Supporting Information Table S2). Similarly, values of [1 − *Q*] for FLC-1250 μmol were also closely correlated with those for CONST-500 μmol, albeit with slightly higher correlation coefficients for 360 s (r^2 = 0.96) than 1200 s (r^2 = 0.89) exposure, reflecting consistently greater induction of nonphotochemical quenching over time (Fig. 2F; Supporting Information Table S2). The slightly lower correlation coefficient for 1200 s compared to 360 s is presumably an outcome of differences in speed of [1 − *Q*] induction across taxa when light dose is increased (Fig. 2D). Together these outcomes verified that FLC-1250 μmol captured changes in quenching capacity that are consistent with those from longer-term protocols, but where the FLC offers a convenient means for rapidly assaying quenching potential alongside retrieval of E_K (Eqs. 1–4).

We next examined whether and how intracolony measurement location influenced photobiological parameterization, and in turn the phenotype identified, using two separate partial colonies of the corymbose species *Acropora tenuis* (At_1, At_2). Replicate samples were systematically examined using FLCs from the colony growing edge to the colony center (*see* Supporting Information Fig. S2). Values of E_K generally increased with distance from colony center to growing edge for FLCs taken for colony At_1 but not colony At_2 (Fig. 3A). However, in spite of this variation of E_K within and between colonies, all LIFT-FRRf parameterization followed extremely conserved trends with E_K for either At_1 or At_2; specifically, decreases in σ_{LHCII}, τ_1, τ_2, and τ_2/PQ_{OX} (Fig. 3B,D–F), and increases in [1 − *C*] (FLC-1250 μmol) and [1 − *Q*] (FLC-1250 μmol) (Fig. 3G,H), which linearly correlated with increasing E_K (r^2 = 0.63–0.87; Supporting Information Table S3). While collectively the reductions observed in light harvesting (σ_{LHCII}), faster electron turnover times (τ_1, τ_2, and τ_2/PQ_{OX}), and more photochemical quenching ([1 − *C*]) are all consistent with acclimation to high light (and hence increases with

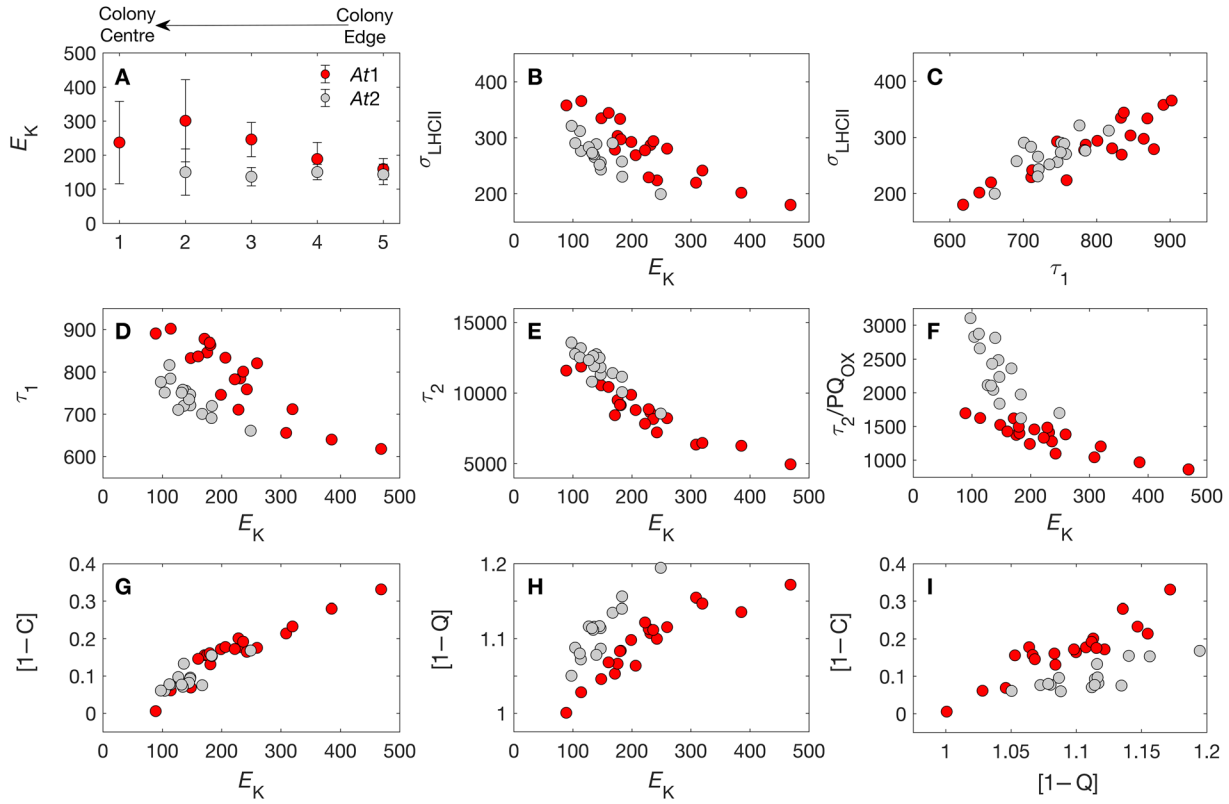

Fig. 3. LIFT-FRRf parameters retrieved from FLC protocols conducted across two different *Acropora tenuis* colonies (At_1, At_2). Panel (**A**) shows the mean ± standard deviation ($n = 4$) light-saturation intensity for PSII photochemistry (E_K, μmol photons m^{-2} s^{-1}; 445 nm) for samples arbitrarily binned into positions sampled systematically from colony center to colony edge (as described in Supporting Information Fig. S2). Panels (**B–J**) compare LIFT-FRRf parameters for all samples collected across the coral surface for either colony: PSII effective cross section (σ_{LHCII}, $Å^2$ quanta^{-1}; 445 + 505 nm) vs. (**B**) E_K, or vs. (**C**) the minimum electron turnover time Q_A to PQ (τ_1, μs); also, (**D**) τ_1, (**E**) τ_2 (minimum time for PQ pool reoxidation; μs), (F) τ_2/PQ_{OX} (minimum downstream transfer of electrons from PQ to PSI; μs), (**G**) extent of photochemical quenching ([1 − C], dimensionless), and (**H**) extent of non-photochemical quenching ([1 − Q], dimensionless), vs. E_K. Also shown is (**I**) [1 − C] vs. [1 − Q]. ANOVA for data in Panel (**A**) and linear regression equations and correlation coefficients for all comparisons (**B–I**) are given in Supporting Information Table S3.

E_K; Hennige et al. 2008, Suggett et al. 2012; Gorbunov and Falkowski 2021), the parallel increase in [1 − Q] (reduced non-photochemical quenching) with E_K (Fig. 3H) is perhaps somewhat counterintuitive. However, the positive correlation of [1 − C] and [1 − Q] with E_K reflect that for a constant FLC protocol, higher light acclimated cells will have less time exposed to light intensities (in this case 1250 μmol photons m^{-2} s^{-1} as the highest intensity for the FLC) that exceed E_K, that is, less time exposed to "excess" excitation energy that particularly builds dynamic [1 − Q]. This can be seen when replotting these comparisons using E_{FLC}/E_K (= 1250/E_K) instead of E_K (Supporting Information Fig. S3). Thus overall, variations in FLC surface sampling location for either colony returned a consistent phenotype of photochemical operation despite Symbiodiniaceae cells optimizing to different absolute light intensities across the colony surface.

Importantly, in contrast to the conserved trends within each colony, linear regression relationships differed between At_1 and At_2 colonies for each of σ_{LHCII}, τ_1, τ_2/PQ_{OX}, and [1 − Q] vs. E_K (Fig. 3; Supporting Information Table S3) indicating different phenotypes; specifically, E_K appears regulated via a phenotype with increased light harvesting, slower Q_A turnover times with less nonphotochemical quenching (but faster PQ to PSI flow), for At_1 relative to At_2. Such FLC-based phenotypes—and notably trade-offs among σ_{LHCII} vs. τ, and [1 − C] vs. [1 − Q] (FLC-1250 μmol)—were further evident when mining of FLC parameterization from samples across all aquarium corals and Symbiodiniaceae culture isolates (Supporting Information Figs. S4, S5; also, *Turbinaria peltata* vs. *Oulophyllia* sp., Fig. 2A–D), an outcome consistent with expression of multiple photo-physiological phenotypes across Symbiodiniaceae taxa ex hospite (*see* Suggett et al. 2015; Goyen et al. 2017) or in hospite (Nitschke et al. 2018).

Field-based phenotyping

FLC-derived E_K values at Opal Reef varied almost 10-fold (~150–1500 μmol photons m^{-2} s^{-1}) across all plating *Acropora* colonies sampled (Fig. 4). Within-species variance of E_K values was generally higher for all plating *Acropora* compared to *E. lamellosa* or *P. verrucosa* (Fig. 4; standard error around the

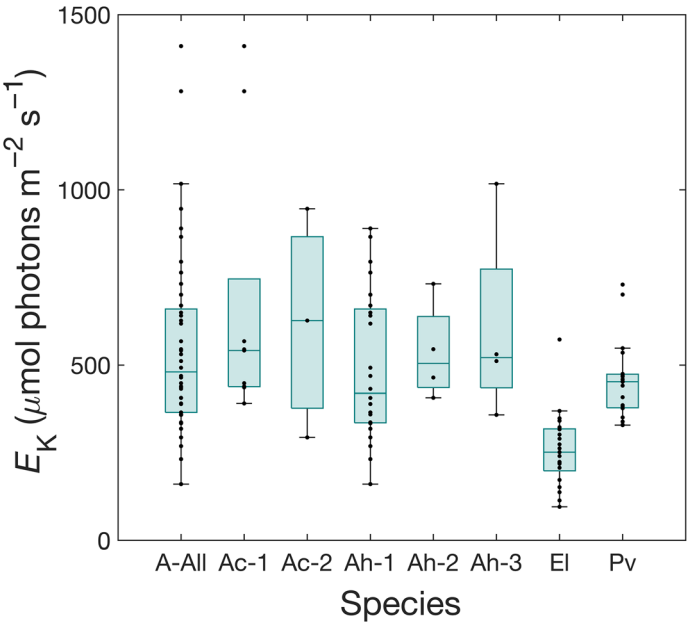

Fig. 4. Range of values retrieved for E_K (μmol photons m^{-2} s^{-1}; 445 nm) across samples at Opal Reef (GBR) for (1) all tabular *Acropora* (A-All; $n = 48$), (2) each tabular *Acropora* morpho-species (*A. cytherea* Ac-1, $n = 9$; Ac-2, $n = 3$; *A. hyacinthus* Ah-1, $n = 24$; Ah-2, $n = 4$; Ah-3, $n = 4$), (3) *Echinopora lamellosa* (El, $n = 20$), and (4) *Pocillopora verrucosa* (Pv, $n = 20$). Data are overlaid onto corresponding boxplots showing median (inner bar), 25% or 75% range (bottom or top of bar), 5% or 95% range (bottom or top whisker).

mean, Table 2). Such greater E_K variance indicates broader light niche plasticity for the plating *Acropora* colonies, a notion consistent with their more diverse topographic distribution compared to *E. lamellosa* or *P. verrucosa* throughout our 2–4 m sampling zone (*see* "Materials and procedures" section). Highest (673 μmol photons m^{-2} s^{-1}) and lowest (259 μmol photons m^{-2} s^{-1}) mean E_K values were observed for *A. cytherea*-2 (Ac-2) and *E. lamellosa*, respectively, with all other species exhibiting intermediary values (~ 450–625 μmol photons m^{-2} s^{-1}); again, the lowest mean E_K values are consistent with the highly cryptic growth topography for this species. Mean values of LIFT-FRRf photo-physiological parameters were largely constant across species other than *E. lamellosa* where F_v/F_m and $[1 - C]$ were lower and τ_1, τ_2, τ_2/PQ_{OX} and $[1 - Q]$ higher than for all other species (Table 2). Differences of these parameters for *E. lamellosa* are consistent with acclimatization to lower light (Gorbunov et al. 2001; Hennige et al. 2008; Suggett et al. 2015), but not the lower F_v/F_m. However, absolute values of F_v/F_m are well established to vary across species of microalgae (including Symbiodiniaceae) (Suggett et al. 2010, 2015), and corals (Levy et al. 2003; Wangpraseurt et al. 2019) via inherently different bio-optical characteristics regulating light harvesting capacity. Within the plating *Acropora*, mean values of LIFT-FRRf parameters were highly variable within and between species, but with notably faster τ_2 (8550 μs) for Ac-1 compared to all others (11,102–15,742 μs) and slower τ_2/PQ_{OX} for Ah-3 (2495 μs) compared to all others (1488–1972 μs) (Table 2).

Large variance of photo-physiological performance within and between species of plating *Acropora* was further evident when comparing the different LIFT-FRRf parameters values against corresponding values of E_K across samples (Fig. 5). While values of σ_{LHCII}, τ_1, τ_2, and τ_2/PQ_{OX} were often higher (and exhibited more variance) with lower E_K, no statistically significant correlations were evident (not shown), in contrast to the same comparisons from the laboratory within-colony assessment (*A. tenuis*; Fig. 3). Such lack of trends between LIFT-FRRf parameters and E_K was apparent when considering all plating *Acropora* species collectively (Fig. 5) as well as each species individually (e.g., *see* red circles for Ah-1 where $n = 24$, Fig. 5), with the exception of $[1 - C]$. Interestingly, values of $[1 - C]$ were positively linearly correlated with E_K ($r^2 = 0.784$, $n = 44$; $p < 0.001$) across all species and samples, indicating highly conserved dependency of the proportion of RCIIs engaged in photochemistry relative to the light intensity of maximum photochemistry. As such, no species-specific phenotypes were evident from considering LIFT-FRRf parameters, even though some parameters appeared to exhibit sample clusters—such as σ_{LHCII} (or $[1 - Q]$) especially at lower E_K values (Fig. 5A,G)—indicative of phenotypic divergence among different isolates of the same species (Suggett et al. 2015, Goyen et al. 2017).

Such species-independent clustering of plating *Acropora* data was further evidenced when subsequently considering all LIFT-FRRf parameters collectively using NMDS (Fig. 6). Specifically, up to four distinct clusters were evident, predominantly driven by differences in turnover time between electron donor-acceptors (τ_1, τ_2, and τ_2/PQ_{OX}) with an additional cluster representing trade-off between decreasing σ_{LHCII} and increasing $[1 - C]$ and $[1 - Q]$ (i.e., less dynamic quenching build-up via the FLC from reduced light harvesting, *see* above).

Comparing the LIFT-FRRf parameters against corresponding E_K values for the other two species (*E. lamellosa*, *P. verrucosa*; Fig. 7) reinforced their respective lower-light vs. higher-light divergence in photo-physiology (Table 2), but again evidenced some within-species variability. Only values for $[1 - C]$ again positively correlated with E_K (Fig. 7F; $r^2 = 0.841$, $n = 20$, $p < 0.001$; *E. lamellosa*; $r^2 = 0.886$, $n = 18$, $p < 0.001$; *P. verrucosa*). While no other LIFT-FRRf parameters were significantly correlated with E_K, values of electron turnover times were of reduced range for *P. verrucosa* (τ_1, ~ 580–810 μs; τ_2, ~ 3900–22,000 μs) compared to *E. lamellosa* (τ_1, ~ 650–1500 μs; τ_2, ~ 4300–32,000 μs) (Fig. 7C,D), but values for σ_{LHCII} (Fig. 7A; ~ 210–500 Å quanta^{-1}) and $[1 - Q]$ (Fig. 7G; ~ 0.871.09) of generally similar range for the two species, despite the higher E_K for *P. verrucosa*. In all, no clear trends were evident within species, which was further reinforced by NMDS clustering based on all LIFT-FRRf parameters where the two species largely clustered separately (Fig. 8). Here the two

Table 2. Mean (± standard error) of photo-physiological properties measured using LIFT-FRRf for colonies of coral species distributed 2–4 m, Opal Reef. Morpho-species are *Acropora cytherea* (Ac-1, $n = 9$; Ac-2, $n = 3$), *A. hyacinthus* (Ah-1, $n = 24$; Ah-2, $n = 4$; Ah-3, $n = 4$), *Echinopora lamellosa* (El, $n = 20$), and *Pocillopora verrucosa* (Pv, $n = 20$). LIFT-FRRf parameters are as for Fig. 3. Results are also shown for ANOVA (MATLAB™ R2020a) comparing each photo-physiological parameter among species, where superscript letter are shown for post hoc Tukey test for $p < 0.05$.

	Species							
	Ac-1	Ac-2	Ah-1	Ah-2	Ah-3	El	Pv	ANOVA
F_v/F_m	0.475 (0.007)^{a}	0.504 (0.004)^{a}	0.474 (0.005)^{a}	0.436 (0.007)^{a,b}	0.486 (0.011)^{a}	0.392 (0.011)^{b}	0.438 (0.010)^{a}	$F = 13.03$ ($p < 0.001$)
σ_{PSII}	108 (9)	105 (13)	120 (4)	121 (9)	122 (15)	117 (4)	126 (3)	$F = 1.22$ ($p = 0.308$)
E_K	673 (129)^{a}	623 (163)^{a,b}	493 (43)^{a,b}	537 (71)^{a,b}	605 (143)^{a,b}	259 (23)^{b}	454 (26)^{a,b}	$F = 5.92$ ($p < 0.001$)
τ_1	698 (42)^{a,b}	639 (26)^{a,b}	795 (49)^{a,b}	917 (146)^{a,b}	774 (112)^{a,b}	965 (66)^{a}	687 (16)^{b}	$F = 3.53$ ($p = 0.004$)
τ_2	8059 (785)^{a}	11,102 (2920)^{a,b}	11,483 (995)^{a,b}	12,090 (2221)^{a,b}	15,742 (1172)^{a,b}	18,072 (1738)^{b}	10,315 (1069)^{a}	$F = 5.30$ ($p < 0.001$)
τ_2/PQ_{OX}	1488 (116)^{a}	1665 (415)^{a}	1972 (217)^{a}	1806 (208)^{a}	2493 (220)^{a,b}	3633 (353)^{b}	1535 (138)^{a}	$F = 8.6$ ($p < 0.001$)
[1 − C]	0.452 (0.036)^{a}	0.405 (0.066)^{a}	0.403 (0.020)^{a}	0.454 (0.021)^{a}	0.477 (0.040)^{a}	0.233 (0.015)^{b}	0.351 (0.013)^{a}	$F = 13.55$ ($p < 0.001$)
[1 − Q]	0.878 (0.022)^{a}	0.905 (0.362)^{a,b}	0.856 (0.017)^{a}	0.789 (0.020)^{a}	0.822 (0.040)^{a}	0.972 (0.013)^{b}	0.946 (0.011)^{b}	$F = 10.55$ ($p < 0.001$)

clusters were again largely driven by variation in turnover time between electron donor-acceptors (τ_1, τ_2, and τ_2/PQ_{OX}), but within-cluster variation driven by the trade-off between increasing σ_{LHCII} and $[1 - Q]$ and decreasing $[1 - C]$.

Together, these field data demonstrate the plating *Acropora* exhibit multiple phenotypes (primarily driven by τ_2/PQ_{OX})—independent of coral taxa—suggesting that broad light niche plasticity (E_K variance) and topographic diversity within the reef habitat sampled is sustained by functional diversity in photobiological performance. In contrast, *E. lamellosa* and *P. verrucosa* exhibited restricted topographic distribution (relatively low-light cryptic vs. high-light exposed, respectively) and reduced light niche plasticity (E_K variance), with separation of diversity in photobiological performance evident between—but not within—species.

Discussion

Global calls to more effectively manage coral reefs have catalyzed development of instrumentation to diagnose changes in coral functional health. In particular, expanding restoration management by coral propagation is driving exploration of new approaches that can discriminate within-species coral functional diversity (Parkinson et al. 2019). Similar needs parallel agriculture where instrumentation based on active Chl *a* fluorescence and protocols are already used to phenotype plant varietals (McAusland et al. 2019; Fernández-Calleja et al. 2020) for selective propagation. While other methods of active fluorometry (e.g., PAM) have gained popularity to coarsely differentiate coral ecotypes within ecological contexts (Nitschke et al. 2018; Camp et al. 2019), novel fluorometer systems that enable greater parameterization of coral photo-physiological traits (Gorbunov et al. 2001; Hoadley and Warner 2017; Leggat et al. 2019; Gorbunov and Falkowski 2021) are yet to be applied to higher throughput phenotyping. Here, we address this gap though a proof-of-concept assessment of using LIFT-FRRf-based parameters as a coral phenotyping method. Using just a relatively restricted set of parameters (Osmond et al. 2017; Keller et al. 2019) and simple screening approach, we resolved various functional types from multiple taxa maintained in aquaria, and for multiple colonies of the same species sampled across a restricted growth environment on the GBR (e.g., plating *Acropora* spp.), demonstrating the potential for active fluorometry to discriminate coral photo-physiological phenotypes.

Our phenotyping approach captures two critical concepts. Firstly, it resolves the dynamic range of light saturation intensity for photochemistry (E_K). Increased characterization of E_K enables improved insight into how changing environmental conditions affect coral function. For example, E_K often changes with light availability (Anthony and Hoegh-Guldberg 2003; Hoogenboom et al. 2006, 2009; Hennige et al. 2008), but also with growth factors such as pH and/or

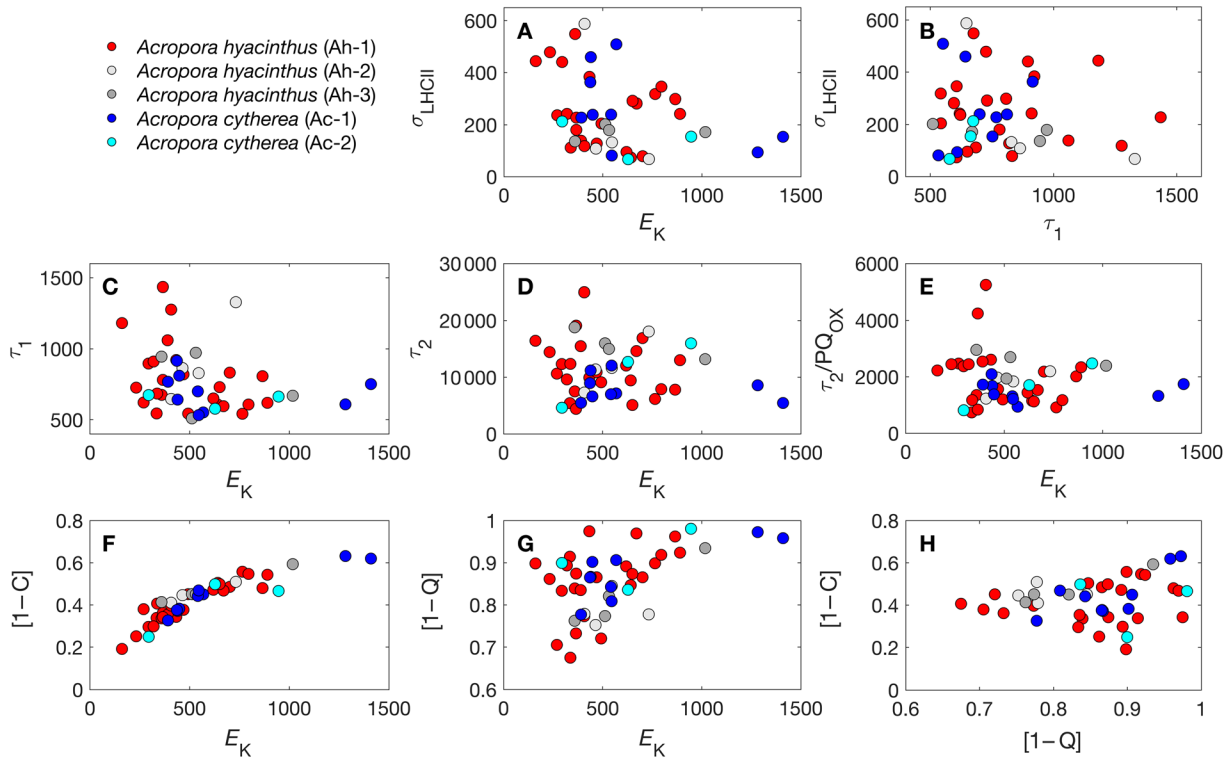

Fig. 5. LIFT-FRRf parameters retrieved from FLC protocols across all plating *Acropora* samples at Opal Reef (GBR) (*A. cytherea* Ac-1, $n = 9$; Ac-2, $n = 3$; *A. hyacinthus* Ah-1, $n = 24$; Ah-2, $n = 4$; Ah-3, $n = 4$): PSII effective cross section (σ_{LHCII}, Å^2 quanta^{-1}; 445 + 505 nm) vs. (**A**) E_K (445 nm), or vs. (**B**) the minimum electron turnover time Q_A to PQ (τ_1, μs); also, (**C**) τ_1, (**D**) τ_2 (minimum time for PQ pool reoxidation; μs), (**E**) τ_2/PQ_{OX} (minimum downstream transfer of electrons from PQ to photosystem I; μs), (**F**) extent of photochemical quenching ([1 − *C*], dimensionless), and (**G**) extent of nonphotochemical quenching ([1 − *Q*], dimensionless), vs. E_K. Also shown is (**H**) [1 − *C*] vs. [1 − *Q*]. Linear correlations were not significant for any of the data plotted, except panel **F** ([1 − *C*] vs. E_K) ($r^2 = 0.784$, $n = 44$, $p < 0.001$).

temperature (Anthony et al. 2008; Nitschke et al. 2018), which typically moderate maximum photosynthesis. As such, deviation of the light dependency of E_K alone can highlight factors other than light that regulate the realized photosynthetic performance (Suggett et al. 2012). Furthermore, changes in E_K via moderations to maximum achievable photosynthesis rates can also inversely correlate with respiration where corals supplement autotrophy with heterotrophy (Anthony and Hoegh-Guldberg 2003; Hoogenboom et al. 2009; Ziegler et al. 2014). Flexibility of E_K (but also other dependent photo-physiological variables) for any given taxa therefore describes the extent of physiological plasticity that underpins observed distributions (e.g., depth, Iglesias-Prieto et al. 2004, Ziegler et al. 2014). For example, corals can overcome distribution restrictions by associating with different "ecotypes" of endosymbiont with inherently different boundaries to photosynthetic performance, including E_K (Iglesias-Prieto et al. 2004). Such attributes suggest that corals with larger dynamic ranges of E_K may therefore be more tolerant to thrive in (or are better adapted to exploit) complex growth environments, which may include multiple endosymbiont associations (Nitschke et al. 2018; Hoadley 2019) or dynamic host properties that can themselves modify E_K (tissue thickness, growth form, etc., Anthony et al. 2005, Wangpraseurt et al. 2019).

Importantly, while we cannot currently resolve the nature of the dynamic ranges for E_K we observed for the different species here (generally greater for the plating *Acropora* species compared to *P. veruccosa* and *E. lamellosa* all sampled from 2 to 4 m depth), these ranges fundamentally provide an emergent signature of the biological and environmental envelopes with which different taxa of interest can grow in complex reef settings. Such knowledge could be central for efforts relocating coral. For example, in situ movement of colonies across reef zones can result in mortality, presumably where factors other than light also change (Lohr et al. 2017) or light-shifts exceed the rate of acclimation (Lohr et al. 2019). Thus, resolving the dynamic range for E_K to indicate phenotypic plasticity may guide more successful transplantation practices in terms of how far and how quickly any given coral taxa (genotype) can be moved for continued propagation and population management.

Secondly, we examined multi-trait photo-physiological phenotypes based on the interplay between factors that ultimately govern E_K variability, light harvesting a_{LHCII} (σ_{LHCII})

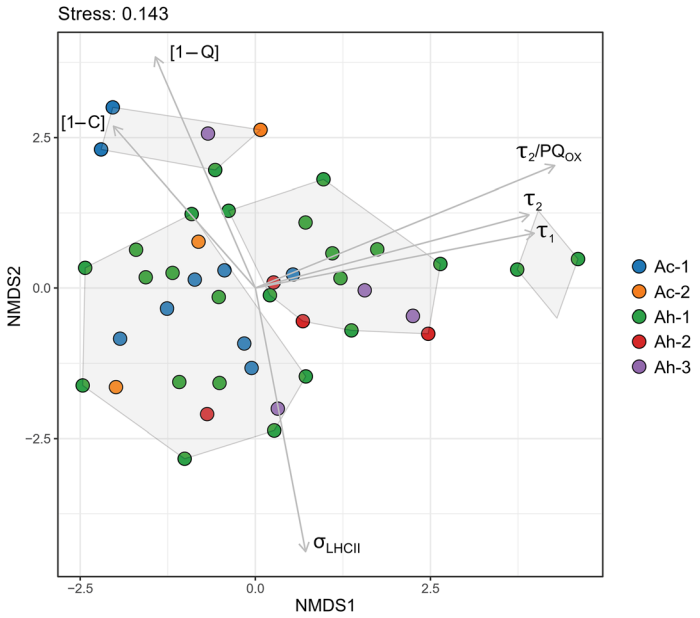

Fig. 6. NMDS based on how all LIFT-FRRf parameters—and in turn E_K—are optimized (σ_{LHCII}, τ_1, τ_2, τ_2/PQ_{OX}) and dynamically regulated ([1 − *C*], [1 − *Q*]) for all samples of plating *Acropora* (*A. cytherea*, Ac-1, Ac-2; *A. hyacinthus*, Ah-1, Ah-2, Ah-3). Significance of individual parameters was assessed against an alpha value of 0.05 (*see* the main text).

vs. light utilization (turnover times, extents of quenching) (Fig. 1). Here, deviations of E_K dependence of these factors (e.g., Fig. 3 contrasting the two *A. tenuis* colonies) inform that inherently different machinery preferentially moderates excitation pressure through PSII. In both laboratory and field-based settings, the only factor that exhibited a consistent relationship with E_K was [1 − C], the extent of "photochemical quenching" (or rather, the proportion of RCIIs engaged in photochemistry). Importantly, the redox state of PSII—and specifically PQ_{OX}—is used as a cue for the extent of photo-acclimation (Escoubas et al. 1995); therefore, the strong and persistent correlations we observed between E_K and [1 − *C*] (but not other factors assessed here) are expected, where [1 − *C*] signals the extent of adjustments to E_K required, but importantly not how this is achieved via the light harvesting and/or utilization machinery. Indeed, adjustments of photo-physiology to transient light availability relative to E_K in corals observed using other active fluorometry platforms has been similarly evidenced through dynamic [1 − *Q*] but highly conserved [1 − *C*] (Hennige et al. 2008, 2011; Suggett et al. 2012). Thus, [1 − *C*] in effect provides a useful "housekeeping" measure for the absolute extent of E_K (light saturation intensity) within multitrait photo-physiological phenotyping assessment.

In the field campaign (Figs. 6, 8), [1 − *Q*] explained some separation of phenotype groups. Variation of [1 − *Q*] does appear to be a strong selecting agent in photosynthetic fitness; for example, of different crop cultivars to CO_2/O_2 availability (McAusland et al. 2019) and also among "ecotypes" of coral endosymbiont maintained as long-term cultures (Suggett et al. 2015). However, such studies identifying [1 − *Q*] used active fluorescence platforms that were unable to resolve parallel activity of the various turnover time components (τ_1, τ_2, τ_2/PQ_{OX}) that the LIFT-FRRf method provided here achieves. In our study, variation of [1 − *Q*] was somewhat secondary to these turnover time components in explaining the phenotype clustering, which in the case of the laboratory-based campaign was limited to [1 − *Q*] driving the spread of samples within each phenotype (Supporting Information Figs. S4, S5). Such an outcome is consistent where turnover kinetic parameters measured by LIFT-FRRf appear highly sensitive to transient environmental perturbation (e.g., coral, Szabó et al. 2017; plants, Keller et al. 2019), and almost certainly reflects the more complete nature with which the different turnover kinetics can describe excitation energy dissipation compared to [1 − *Q*] (Hughes et al. 2018, Keller et al. 2019; Fig. 1). Consequently, the combined nature of [1 − *Q*] with τ_1, τ_2, and/or τ_2/PQ_{OX} expands the range of observable phenotypes beyond that achievable using [1 − *Q*]. As such, other fluorometer protocols such as conventional PAM-based configurations that only resolve amplitude (e.g., F_v/F_m, [1 − C], [1 − *Q*], FLC-based E_K) and not kinetic (σ_{LHCII}, τ_1, τ_2, PQ_{OX}, etc.) parameters may prove far less powerful for discriminating photo-physiological phenotypes, but remains to be tested in future. With this in mind, future analysis using protocols that only retrieve amplitude-based parameters could probe whether and how unbounded, but time-resolved, descriptions of non-photochemical quenching (e.g., $NPQ = [F_m - F_m']/F_m'$) potentially offset limitations of not capturing kinetic parameters for resolving phenotypes.

Intriguingly in our study, of the various kinetic turnover parameters, τ_2/PQ_{OX} was often the dominant vector driving cluster separation, suggesting separation phenotypes of plating *Acropora* species—or indeed *E. lamellosa* vs. *P. verrucosa*—by divergent activity downstream of PSII (Szabó et al. 2017; Hughes et al. 2018). This finding supports previous observations of differential reliance on PSI for moderating excess energy flows among endosymbionts in culture (Roberty et al. 2014) or in hospite of corals (Szabó et al. 2017; Vega de Luna et al. 2020; but *see* Hoogenboom et al. 2012), and clearly warrants more targeted investigation in future. While we cannot resolve the underlying basis for the alternate phenotypes of *Acropora* retrieved via LIFT-FRRf here, which were dispersed across different *Acropora* species (or morpho-species), it is possibly an outcome of known plasticity of association between these various hosts and alternate Symbiodiniaceae taxa (e.g., *A. cytherea*, Rouzé et al. 2019). Regardless, our LIFT-FRRf assay would demonstrate that at least four photo-physiological phenotypes (multitrait clusters, Fig. 6) are evident across the *Acropora* species (morpho-species) examined here—and so it would be desirable that coral propagation efforts ensure this full suite of functional diversity is retained.

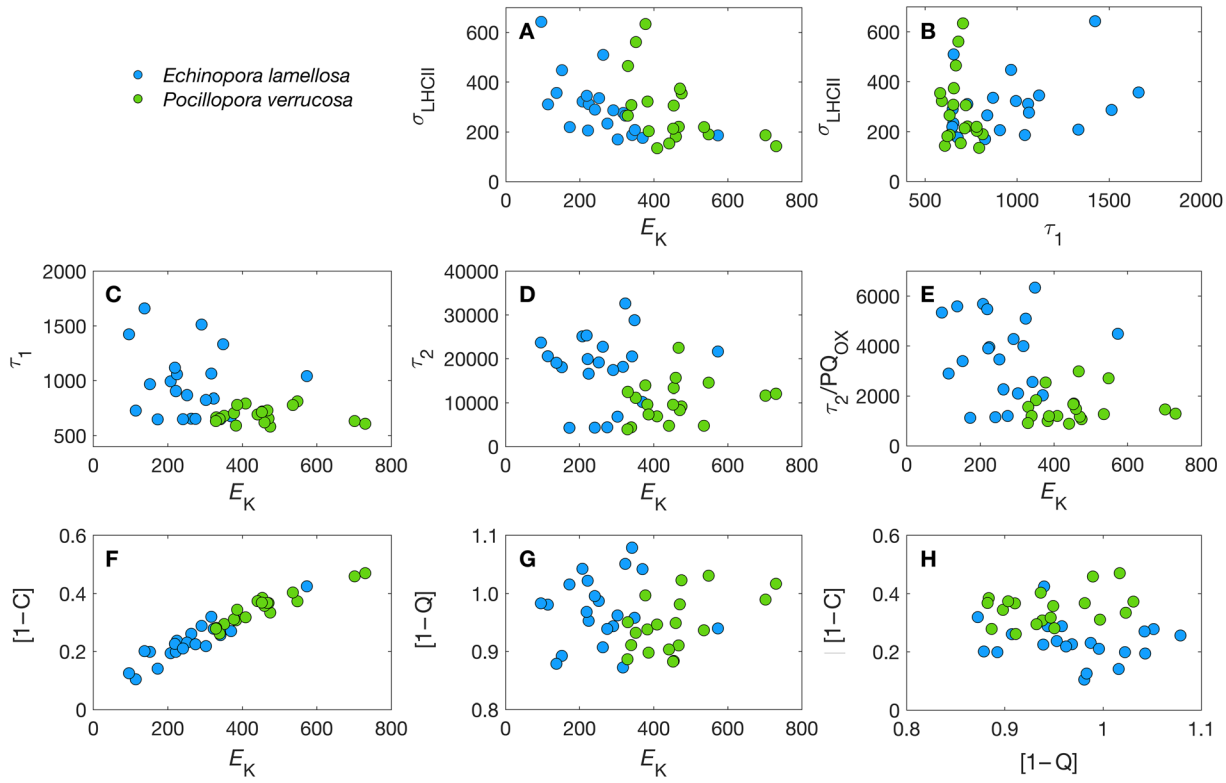

Fig. 7. LIFT-FRRf parameters retrieved from FLC protocols across all *Echinopora lamellosa* and *Pocillopora verrucosa* samples (each $n = 20$) at Opal Reef (GBR): panels are as for Fig. 5. Linear correlations were not significant for any of the data plotted—either collectively as each species independently—except panel **F** ([1 − *C*] vs. E_K) ($r^2 = 0.841$, $p < 0.001$, *E. lamellosa*; $r^2 = 0.886$, $p < 0.001$, *P. verrucosa*).

Our proof-of-concept assessment here describes different coral phenotypes based on photo-physiological performance. From the photochemical traits selected (Fig. 1), field-based screening resolved at least four different phenotypes (as four multitrait clusters, Fig. 6) of plating *Acropora* alone (and more phenotypes/clusters than observed for our laboratory work using diverse coral species maintained under relatively environmentally static aquarium conditions), which was consistent with capacity for greater light niche plasticity and broader within-habitat topographic distribution at 2–4 m depth. As such, LIFT-FRRf phenotyping would appear promising as a convenient tool to rapidly resolve fine scale differences in niche partitioning of coral photo-physiological functional performance, and a means to identify functionally diverse taxa. Both factors could provide novel capacity to support coral propagation efforts wishing to select and track functional diversity, as well as better match growing (or outplanting) locations to photo-physiological performance optima.

Comments and recommendations

Use of LIFT-FRRf as a coral phenotyping platform here exploited relatively standard protocols and parameters that have been previously established for higher plants (Kolber et al. 2005; Osmond et al. 2017, 2019; Keller et al. 2019). Clearly, to optimize this—or indeed any other Chl *a* fluorometer—to better discriminate coral phenotypic functional diversity will require a series of conceptual, technical, and operational recommendations to improve applicability (and guide further development) of the approach (summarized in Table 3):

(1) Deeper physiological parameterization—We used a relatively restricted selection of LIFT-FRRf parameters here (both amplitude-based F_v/F_m, [1 − *C*], [1 − *Q*], FLC-based E_K, and kinetic-based σ_{PSII}, τ_1, τ_2, PQ_{OX}), which resulted in discrimination of several phenotypes (Figs. 6, 8; also Supporting Information Fig. 5). Clearly, exploration of more traits will be necessary to further maximize the extent of phenotype retrieval possible (Kuhlgert et al. 2016; Keller et al. 2019), and/or provide an improved means for machine learning to reduce distinct physiologies—which may include handling multiple autocorrelated traits—into robust phenotypes (Kuhlgert et al. 2016; Yao et al. 2018). Novel Chl *a* fluorescence induction and parameterization approaches including LIFT-FRRf still have a wealth of parameters that can be examined: notably, further discrete photo-physiological traits (e.g., carotenoid and donor-side quenching; Kolber

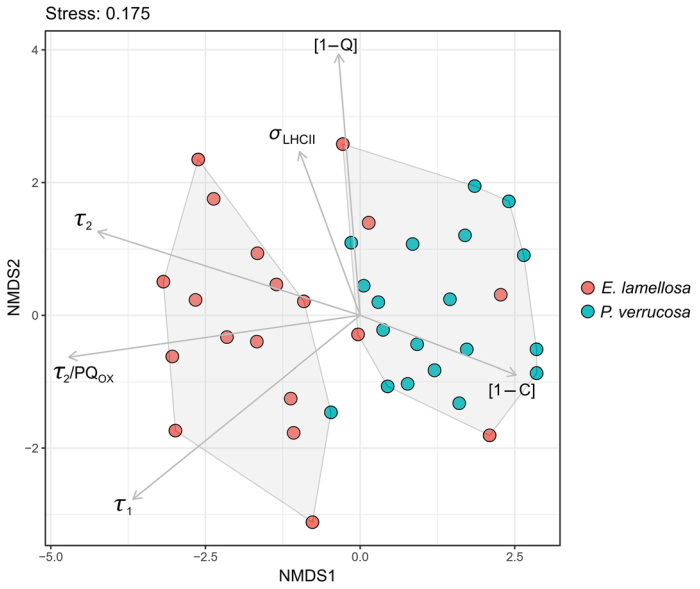

Fig. 8. NMDS based on how all LIFT-FRRf parameters—and in turn E_K—are optimized (σ_{LHCII}, τ_1, τ_2, τ_2/PQ_{OX}) and dynamically regulated ([1 − *C*], [1 − Q]) for all *Echinopora lamellosa* and *Pocillopora verrucosa*. Significance of individual parameters was assessed against an alpha value of 0.05 (*see* the main text).

et al. 1998, Osmond et al. 2017, Keller et al. 2019), retrieval of E_K from "instantaneous" induction-decay measurements (as opposed to derived from FLC) (Gorbunov and Falkowski 2021), adoption of more diverse excitation-emission spectra indicative of immunological factors (Bollati et al. 2020), microbiome entities beyond Symbiodiniaceae (Leggat et al. 2019), and optical thickness/packaging (Boatman et al. 2019). Including such factors may involve bio-optical reconfiguration of existing platforms, and could conceivably extend to more sophisticated bio-optical platforms that align Chl *a* fluorescence with other bio-optical approaches, such as Raman spectroscopy to resolve calcification dynamics (DeCarlo et al. 2019). Ultimately different configurations may depend on the phenotyping goals and traits of interest.

(2) Improved operation for high-throughput screening *in situ*—Ultimately high throughput capacity for screening rests on speed of sample turnover, which is currently slowed by the need to invasively sample and process coral biopsies ex situ. Evolving Chl *a* fluorescence induction platforms to retrieve data in water, as already possible achieved for other FRRf-type diving instruments (Gorbunov et al. 2001; Gorbunov and Falkowski 2021), supported by computational software to rapidly assess traits to retrieve phenotypes of interest (Kuhlgert et al. 2016, Yao et al. 2018), are needed to progress instruments from research tools into sensors capable of providing meaningful and rapid decisions to nonspecialist users. While novel algorithms using single inductions may overcome the need for more time consuming FLCs to retrieve E_K (Gorbunov and Falkowski 2021), knowledge of quenching dynamics currently appear to be key traits informing discrimination of phenotypes—and therefore still require relatively prolonged actinic light protocols—unless empirical algorithms are further explored to retrieve quenching extents from short induction protocols (beyond that here, Fig. 2). Instantaneous protocols collected from the same sample over different times of day may capture dynamic quenching states (Gorbunov et al. 2001), whereas contrasting day vs. night could parameterize tissue contraction (Levy et al. 2003) to aid resolving packaging effects. Such examples highlight that repeat measurements over time on individual colonies may therefore be a critical operational step—not only would they carry benefits toward more validation (or deeper physiological characterization) of phenotypes but in themselves provide novel insight into fine scale coral performance dynamics:

(3) Phenotype validation 1: Capturing phenotype plasticity—LIFT-FRRf assessments currently yield photophysiological phenotypic signatures of Symbiodiniaceae community performance, which in our proof-of-concept here demonstrated how the same coral host can exhibit functional diversity over small reef spatial scales. However, how such alternate phenotypes reflect changes in the predominant Symbiodiniaceae taxa (as opposed to other adaptive processes) is unclear. Corals hosting different Symbiodiniaceae taxa is well evidenced as corals acclimatize to altered reef environments and/or time (Kemp et al. 2014; Camp et al. 2019), which in turn parallels with very different Chl *a* fluorescence signatures (Nitschke et al. 2018; Camp et al. 2019). Thus, characterizing the dynamic range of phenotype expression over space and time is critical to define the adaptive niche of any given host species of interest, and so resolve evolutionary divergent or convergent functional strategies (Suggett et al. 2015). Ensuring high-throughput characterization across life history stages, where larval and/or juvenile corals can be particularly promiscuous in terms of symbiont association (Quigley et al. 2017), may in turn provide a means to better understand compatibility (and hence survivorship potential) between early life history stages and reef microenvironment. Similarly, intensive within-colony characterization may be used to predict where optical niches produced by self-shading enable coexistence of multiple Symbiodiniaceae taxa within a single coral colony (Ulstrup et al. 2007; Kemp et al. 2014).

(4) Phenotype validation II: Develop deeper insight of phenotypes—While characterizing any given photophysiological phenotype(s) provides the operational approach for future targeted selection required for propagation, a critical—and perhaps most fundamental—step is gaining deeper insight into the system biology shaping these phenotypes; in other words, how does the phenotype reflect the real properties of interest? For example, in our proof-of-concept, what is driving changes in turnover time constants (and notably τ_2/PQ_{OX}) relative to E_K?—that is factors h particularly key

Table 3. Summary of development areas recommended (*see* the main text) to progress active Chl *a* fluorometry-based coral phenotyping platforms.

Development area	Solution required	Benefits gained
Technical	In water capability	More immediate signature retrieval. Remove need to extract samples (permitting) and/or introduce sample handing effects.
	Additional and/or more tailored bio-optical information (multi excitation-emission)	Include chromatic information to describe parallel responses of host and/or other microbial entitles (e.g., endoliths). Include bio-optical descriptors to better quantify pigment packaging (and in turn improve photo-physiological depth, e.g., [RCII] to determine a_{LHCII} from σ_{LHCII}).
	Computational (machine learning) for "deeper parameterization" and phenotype retrieval.	Deeper physiological insight of LIFT-FRRf retrieved parameters. Distil complex multidimensional responses (within minimum degrees of freedom) to a desired phenotype "signature" that can be employed by nonspecialists.
Operational	"Instantaneous" retrieval of E_K and other photo-physiological metrics.	Further increase speed of data acquisition.
	Multiple samples per colony.	Overcome uncertainties associated with inherent intracolony variance in niche space.
	Multiple samples per time of day.	Overcome uncertainties associated with light-history effects on photo-physiology via "instantaneous" measures. Use as a possible means to gauge variance on photo-physiology induced via tissue contraction (packaging).
Conceptual	Understand how phenotypic variability can be explained by Symbiodiniaceae species/other holobiont factors, and how this reflects changes of environment, life history, etc.	Resolve niche width of performance based on changes to host-symbiont factors (guiding where species can/cannot be propagated). Aid refining phenotype for real time "decision making" for propagation.
	Resolve photo-physiological phenotype with independent assessment (e.g., functional genomics platforms, conventional assays, e.g., respirometry, growth, etc.).	Aligns photo-physiology (phenotype) with other specific attributes of interest for selective propagation. Aid refining phenotype for real time "decision making" for propagation.

in discriminating our plating *Acropora* phenotypes—and how does this potentially govern growth and survivorship performance? Recent studies have begun to reconcile how changes in coral (Symbiodiniaceae) photo-physiological expression and function correspond to the underlying shifts in coral metabolism (e.g., through coupled metabolomics; Lohr et al. 2019), or parallel to reconfigured metabolic strategies of the host (e.g., respirometry, calcification; Camp et al. 2019). As such, robustness of rapid and convenient phenotype discrimination using bio-optics will rest on developing both mechanistic and empirical descriptors of symbiont-host functioning, including parallel measures of ecological fitness outcomes (growth, survivorship etc.), so as to effectively target coral phenotypes that carry high priority for reef conservation or restoration efforts.

In summary, our proof-of-concept application of LIFT-FRR fluorometry here considers how the rapid development of Chl *a* induction approaches—including LIFT-FRRf—for phenotyping plants (Yao et al. 2018; Keller et al. 2019; McAusland et al. 2019) can be applied to coral. We have adopted previous insight from FRRf development for examining corals (Gorbunov et al. 2001, Gorbunov and Falkowski 2021) and Symbiodiniaceae functional diversity (Suggett et al. 2015; Goyen et al. 2017; Nitschke et al. 2018) to assess how phenotypes of photo-physiological performance can be retrieved from diverse coral taxa in the laboratory and the field. Fundamentally, the approach (and recommended roadmap for future development) provides a means for higher resolution assessment for how coral photosynthetic functioning changes over space and time in complex reef environments and in near-real time. We propose that such a phenotyping approach could provide a novel means to noninvasively identify/select phenotypes to aid management, maintenance and propagation of coral populations.

References

Anthony, K. R. N., and O. Hoegh-Guldberg. 2003. Variation in coral photosynthesis, respiration and growth characteristics in contrasting light microhabitats: An analogue to plants in forest gaps and understoreys? Funct. Ecol. **17**: 246–259. doi:10.1046/j.1365-2435.2003.00731.x

Anthony, K. R. N., P. V. Ridd, A. R. Orpin, P. Larcombe, and J. Lough. 2004. Temporal variation of light availability in coastal benthic habitats: Effects of clouds, turbidity, and tides. Limnol. Oceanogr. **49**: 2201–2211. doi:10.4319/lo.2004.49.6.2201

Anthony, K. R. N., M. O. Hoogenboom, and S. R. Connolly. 2005. Adaptive variation in coral geometry and the optimization of internal colony light climates. Funct. Ecol. **19**: 17–26. doi:10.1111/j.0269-8463.2005.00925.x

Anthony, K. R. N., D. I. Kline, G. Diaz-Pulido, S. Dove, and O. Hoegh-Guldberg. 2008. Ocean acidification causes bleaching and productivity loss in coral reef builders. Proc. Natl. Acad. Sci. USA **105**: 17442–17446. doi:10.1073/pnas.0804478105

Baums, I. B., and others. 2019. Considerations for maximizing the adaptive potential of restored coral populations in the western Atlantic. Ecol. Appl. **29**: e01978. doi:10.1002/eap.1978

Boatman, T. G., R. J. Geider, and K. Oxborough. 2019. Improving the accuracy of single turnover active fluorometry (STAF) for the estimation of phytoplankton primary productivity (PhytoPP). Front. Mar. Sci. **6**: 319. doi:10.3389/fmars.2019.00319

Bollati, E., C. D'Angelo, R. Alderdice, M. Pratchett, M. Ziegler, and J. Wiedenmann. 2020. Optical feedback loop involving dinoflagellate symbiont and scleractinian host drives colorful coral bleaching. Curr. Biol. **30**: 2433–2445.e3. doi:10.1016/j.cub.2020.04.055

Boström-Einarsson, L., and others. 2020. Coral restoration—a systematic review of current methods, successes, failures and future directions. PLoS One **15**: e0226631. doi:10.1371/journal.pone.0226631

Camp, E. F., J. Edmondson, A. Doheny, J. Rumney, A. J. Grima, A. Huete, and D. J. Suggett. 2019. Mangrove lagoons of the Great Barrier Reef support coral populations persisting under extreme environmental conditions. Mar. Ecol. Prog. Ser. **625**: 1–14. doi:10.3354/meps13073

Charrad, M. N., N. Ghazzali, V. Boiteau, and A. Niknafs. 2014. NbClust: An R package for determining the relevant number of clusters in a data set. J. Stat. Softw. **61**: 1–36. doi:10.18637/jss.v061.i06

Cleves, P. A., A. I. Tinoco, J. Bradford, D. Perrin, L. K. Bay, and J. R. Pringle. 2020. Reduced thermal tolerance in a coral carrying CRISPR-induced mutations in the gene for a heat-shock transcription factor. Proc. Natl. Acad. Sci. USA **117**: 28899–28905. doi:10.1073/pnas.1920779117

DeCarlo, T. M., and others. 2019. Investigating marine biocalcification mechanisms in a changing ocean with in vivo and high-resolution ex vivo Raman spectroscopy. Glob. Chang. Biol. **25**: 1877–1888. doi:10.1111/gcb.14579

Elzhov, T.V., K. M. Mullen, A. N. Spiess, and B. Bolker. 2013. minpack.lm: R interface to the Levenberg-Marquardt nonlinear least-squares algorithm found in MINPACK, plus support for bounds. R package version 1.1-8. Available from http://CRAN.Rproject.org/package=minpack.lm.

Escoubas, J. M., M. Lomas, J. LaRoche, and P. G. Falkowski. 1995. Light intensity regulation of cab gene transcription is signaled by the redox state of the plastoquinone pool. Proc. Natl. Acad. Sci. USA **92**: 10237–10241. doi:10.1073/pnas.92.22.10237

Fernández-Calleja, M., A. Monteagudo, A. M. Casas, C. Boutin, P. A. Pin, F. Morales, and E. Igartua. 2020. Rapid on-site phenotyping via field fluorimeter detects differences in photosynthetic performance in a hybrid—Parent barley germplasm set. Sensors **20**: 1486. doi:10.3390/s20051486

Gorbunov, M. Y., Z. S. Kolber, M. P. Lesser, and P. G. Falkowski. 2001. Photosynthesis and photoprotection in symbiotic corals. Limnol. Oceanogr. **46**: 75–85. doi:10.4319/lo.2001.46.1.0075

Gorbunov, M. Y., and P. G. Falkowski. 2021. Using chlorophyll fluorescence kinetics to determine photosynthesis in aquatic ecosystems. Limnol. Oceanogr. **66**: 1–13. doi:10.1002/lno.11581

Goyen, S., M. Pernice, M. Szabó, M. E. Warner, P. J. Ralph, and D. J. Suggett. 2017. A molecular physiology basis for functional diversity of hydrogen peroxide production amongst *Symbiodinium* spp. (Dinophyceae). Mar. Biol. **164**: 46. doi:10.1007/s00227-017-3073-5

Hennige, S., D. Smith, R. Perkins, M. Consalvey, D. Paterson, and D. J. Suggett. 2008. Photoacclimation, growth and distribution of massive coral species in clear and turbid waters. Mar. Ecol. Prog. Ser. **369**: 77–88. doi:10.3354/meps07612

Hennige, S. J., M. P. McGinley, A. G. Grottoli, and M. E. Warner. 2011. Photoinhibition of *Symbiodinium* spp. within the reef corals *Montastraea faveolata* and *Porites astreoides*: Implications for coral bleaching. Mar. Biol. **158**: 2515–2526. doi:10.1007/s00227-011-1752-1

Hoadley, K. D., and M. E. Warner. 2017. Use of open source hardware and software platforms to quantify spectrally dependent differences in photochemical efficiency and functional absorption cross section within the dinoflagellate *Symbiodinium* spp. Front. Mar. Sci. **4**: 365. doi:10.3389/fmars.2017.00365

Hoadley, K. D. others 2019. Host–symbiont combinations dictate the photo-physiological response of reef-building corals to thermal stress. Sci. Rep. **9**: 1–15. doi:10.1038/s41598-019-46412-4

Hoogenboom, M. O., K. R. N. Anthony, and S. R. Connolly. 2006. Energetic cost of photoinhibition in corals. Mar. Ecol. Prog. Ser. **313**: 1–12. doi:10.3354/meps313001

Hoogenboom, M. O., S. R. Connolly, and K. R. N. Anthony. 2009. Effects of photoacclimation on the light niche of corals: A process-based approach. Mar. Biol. **156**: 2493–2503. doi:10.1007/s00227-009-1274-2

Hoogenboom, M. O., D. A. Campbell, E. Beraud, K. DeZeeuw, and C. Ferrier-Pagès. 2012. Effects of light, food availability and temperature stress on the function of photosystem II and photosystem I of coral symbionts. PLoS One **7**: e30167. doi:10.1371/journal.pone.0030167

Hoogenboom, M. O., and others. 2017. Environmental drivers of variation in bleaching severity of Acropora species during an extreme thermal anomaly. Front. Mar. Sci. **4**: 376. doi:10.3389/fmars.2017.00376

Howlett, L., E. F. Camp, J. Edmondson, N. Henderson, and D. J. Suggett. 2021. Coral growth, survivorship and return-on-effort within nurseries at high-value sites on the Great Barrier Reef. PLoS One **16**: e0244961. doi:10.1371/journal.pone.0244961

Hughes, T. P., and others. 2017. Coral reefs in the Anthropocene. Nature **546**: 82–90. doi:10.1038/nature22901

Hughes, D. J., and others. 2018. Roadmaps and detours: Active chlorophyll-a assessments of primary productivity across marine and freshwater systems. Environ. Sci. Technol. **52**: 12039–12054. doi:10.1021/acs.est.8b03488

Iglesias-Prieto, R., V. H. Beltrán, T. C. LaJeunesse, H. Reyes-Bonilla, and P. E. Thomé. 2004. Different algal symbionts explain the vertical distribution of dominant reef corals in the eastern Pacific. Proc. R. Soc. B Biol. Sci. **271**: 1757–1763. doi:10.1098/rspb.2004.2757

Kaniewska, P., K. R. N. Anthony, E. M. Sampayo, P. R. Campbell, and O. Hoegh-Guldberg. 2014. Implications of geometric plasticity for maximizing photosynthesis in branching corals. Mar. Biol. **161**: 313–328. doi:10.1007/s00227-013-2336-z

Keller, B., and others. 2019. Maximum fluorescence and electron transport kinetics determined by light-induced fluorescence transients (LIFT) for photosynthesis phenotyping. Photosynth. Res. **140**: 221–233. doi:10.1007/s11120-018-0594-9

Kemp, D. W., X. Hernandez-Pech, R. Iglesias-Prieto, W. K. Fitt, and G. W. Schmidt. 2014. Community dynamics and physiology of *Symbiodinium* spp. before, during, and after a coral bleaching event. Limnol. Oceanogr. **59**: 788–797. doi:10.4319/lo.2014.59.3.0788

Kolber, Z. S., O. Prášil, and P. G. Falkowski. 1998. Measurements of variable chlorophyll fluorescence using fast repetition rate techniques: Defining methodology and experimental protocols. Biochim. Biophys. Acta Bioenerg. **1367**: 88–106. doi:10.1016/S0005-2728(98)00135-2

Kolber, Z., D. Klimov, G. Ananyev, U. Rascher, J. Berry, and B. Osmond. 2005. Measuring photosynthetic parameters at a distance: Laser induced fluorescence transient (LIFT) method for remote measurements of photosynthesis in terrestrial vegetation. Photosynth. Res. **84**: 121–129. doi:10.1007/s11120-005-5092-1

Kuhlgert, S., and others. 2016. MultispeQ Beta: A tool for large-scale plant phenotyping connected to the open photosynQ network. R. Soc. Open Sci. **3**: 160592. doi:10.1098/rsos.160592

Ladner, J. T., and S. R. Palumbi. 2012. Extensive sympatry, cryptic diversity and introgression throughout the geographic distribution of two coral species complexes. Mol. Ecol. **21**: 2224–2238. doi:10.1111/j.1365-294X.2012.05528.x

Leggat, W. P., and others. 2019. Rapid coral decay is associated with marine heatwave mortality events on reefs. Curr. Biol. **29**: 2723–2730.e4. doi:10.1016/j.cub.2019.06.077

Levin, R. A., D. J. Suggett, M. R. Nitschke, M. J. H. van Oppen, and P. D. Steinberg. 2017. Expanding the *Symbiodinium* (Dinophyceae, Suessiales) toolkit through protoplast technology. J. Eukaryot. Microbiol. **64**: 588–597. doi:10.1111/jeu.12393

Levy, O., Z. Dubinsky, and Y. Achituv. 2003. Photobehavior of stony corals: Responses to light spectra and intensity. J. Exp. Biol. **206**: 4041–4049. doi:10.1242/jeb.00622

Lohr, K. E., A. A. Cook McNab, C. Manfrino, and J. T. Patterson. 2017. Assessment of wild and restored staghorn coral *Acropora cervicornis* across three reef zones in the Cayman Islands. Reg. Stud. Mar. Sci. **9**: 1–8. doi:10.1016/j.rsma.2016.11.003

Lohr, K. E., E. F. Camp, U. Kuzhiumparambil, A. Lutz, W. Leggat, J. T. Patterson, and D. J. Suggett. 2019. Resolving coral photoacclimation dynamics through coupled photophysiological and metabolomic profiling. J. Exp. Biol. **222**: jeb195982. doi:10.1242/jeb.195982

McAusland, L., J. A. Atkinson, T. Lawson, and E. H. Murchie. 2019. High throughput procedure utilising chlorophyll fluorescence imaging to phenotype dynamic photosynthesis and photoprotection in leaves under controlled gaseous conditions. Plant Methods **15**: 109. doi:10.1186/s13007-019-0485-x

Morikawa, M. K., and S. R. Palumbi. 2019. Using naturally occurring climate resilient corals to construct bleaching-resistant nurseries. Proc. Natl. Acad. Sci. USA **116**: 10586–10591. doi:10.1073/pnas.1721415116

Nitschke, M. R., S. G. Gardner, S. Goyen, L. Fujise, E. F. Camp, P. J. Ralph, and D. J. Suggett. 2018. Utility of photochemical traits as diagnostics of thermal tolerance amongst Great Barrier Reef corals. Front. Mar. Sci. **5**: 45. doi:10.3389/fmars.2018.00045

Oksanen, J. & others 2015. The vegan package. Community ecology package. R package version 2.3-2. Available from http://CRAN.R-project.org/package=vegan

Osmond, B., W. S. Chow, R. Wyber, A. Zavafer, B. Keller, B. J. Pogson, and S. A. Robinson. 2017. Relative functional and optical absorption cross-sections of PSII and other photosynthetic parameters monitored *in situ*, at a distance with a time resolution of a few seconds, using a prototype light

induced fluorescence transient (LIFT) device. Funct. Plant Biol. **44**: 985–1006. doi:10.1071/FP17024

Osmond, B., W. S. Chow, B. J. Pogson, and S. A. Robinson. 2019. Probing functional and optical cross-sections of PSII in leaves during state transitions using fast repetition rate light induced fluorescence transients. Funct. Plant Biol. **46**: 567–583. doi:10.1071/FP18054

Oxborough, K., C. M. Moore, D. J. Suggett, T. Lawson, H. G. Chan, and R. J. Geider. 2012. Direct estimation of functional PSII reaction center concentration and PSII electron flux on a volume basis: A new approach to the analysis of fast repetition rate fluorometry (FRRf) data. Limnol. Oceanogr. Methods **10**: 142–154. doi:10.4319/lom.2012.10.142

Padfield, D., G. Yvon-Durocher, A. Buckling, S. Jennings, and G. Yvon-Durocher. 2016. Rapid evolution of metabolic traits explains thermal adaptation in phytoplankton. Ecol. Lett. **19**: 133–142. doi:10.1111/ele.12545

Parkinson, J. E., and others. 2019. Molecular tools for coral reef restoration: Beyond biomarker discovery. Conserv. Lett. **13**: e12687. doi:10.1111/conl.12687

Peterson, R. A., and J. E. Cavanaugh. 2020. Ordered quantile normalization: A semiparametric transformation built for the cross-validation era. J. Appl. Stat. **47**: 2312–2327. doi:10.1080/02664763.2019.1630372

Pleban, J. R., C. R. Guadagno, D. S. MacKay, C. Weinig, and B. E. Ewers. 2020. Rapid chlorophyll a fluorescence light response curves mechanistically inform photosynthesis modeling. Plant Physiol. **183**: 602–619. doi:10.1104/pp.19.00375

Quigley, K. M., B. L. Willis, and L. K. Bay. 2017. Heritability of the *Symbiodinium* community in vertically-and horizontally-transmitting broadcast spawning corals. Sci. Rep. **7**: 866. doi:10.1038/s41598-017-08179-4

Roberty, S., B. Bailleul, N. Berne, F. Franck, and P. Cardol. 2014. PSI Mehler reaction is the main alternative photosynthetic electron pathway in *Symbiodinium* sp., symbiotic dinoflagellates of cnidarians. New Phytol. **204**: 81–91. doi:10.1111/nph.12903

Roberty, S., E. Béraud, R. Grover, and C. Ferrier-Pagès. 2020. Coral productivity is co-limited by bicarbonate and ammonium availability. Microorganisms **8**: 640. doi:10.3390/microorganisms8050640

Ros, M., E. F. Camp, D. J. Hughes, J. R. Crosswell, M. E. Warner, W. P. Leggat, and D. J. Suggett. 2020. Unlocking the black-box of inorganic carbon-uptake and utilization strategies among coral endosymbionts (Symbiodiniaceae). Limnol. Oceanogr. **65**: 1747–1763. doi:10.1002/lno.11416

Rouzé, H., G. Lecellier, X. Pochon, G. Torda, and V. Berteaux-Lecellier. 2019. Unique quantitative Symbiodiniaceae signature of coral colonies revealed through spatio-temporal survey in Moorea. Sci. Rep. **9**: 1–11. doi:10.1038/s41598-019-44017-5

Schuback, N., and others. 2021. Single-turnover variable chlorophyll fluorescence as a tool for assessing phytoplankton photosynthesis and primary productivity: Opportunities, caveats and recommendations. Front. Mar. Sci. **8**: 690607. doi:10.3389/fmars.2021.690607

Suggett, D. J., K. Oxborough, N. R. Baker, H. L. Macintyre, T. M. Kana, and R. J. Geider. 2003. Fast repetition rate and pulse amplitude modulation chlorophyll a fluorescence measurements for assessment of photosynthetic electron transport in marine phytoplankton. Eur. J. Phycol. **38**: 371–384. doi:10.1080/0967026031000161265 5

Suggett, D. J., H. L. Macintyre, and R. J. Geider. 2004. Evaluation of biophysical and optical determinations of light absorption by photosystem II in phytoplankton. Limnol. Oceanogr. Methods **2**: 316–332. doi:10.4319/lom.2004.2.316

Suggett, D. J., C. M. Moore, and R. J. Geider. 2010. Estimating aquatic productivity from active fluorescence measurements, p. 103–127. *In* Chlorophyll *a* fluorescence in aquatic sciences: Methods and applications. Springer.

Suggett, D. J., R. K. P. Kikuchi, M. D. M. Oliveira, S. Spanó, R. Carvalho, and D. J. Smith. 2012. Photobiology of corals from Brazil's near-shore marginal reefs of Abrolhos. Mar. Biol. **159**: 1461–1473. doi:10.1007/s00227-012-1925-6

Suggett, D. J., S. Goyen, C. Evenhuis, M. Szabó, D. T. Pettay, M. E. Warner, and P. J. Ralph. 2015. Functional diversity of photobiological traits within the genus *Symbiodinium* appears to be governed by the interaction of cell size with cladal designation. New Phytol. **208**: 370–381. doi:10.1111/nph.13483

Suggett, D. J., M. E. Warner, and W. Leggat. 2017. Symbiotic dinoflagellate functional diversity mediates coral survival under ecological crisis. Trends Ecol. Evol. **32**: 903–745. doi:10.1016/J.TREE.2017.07.013

Suggett, D. J., J. Edmondson, L. Howlett, and E. F. Camp. 2020. Coralclip®: A low-cost solution for rapid and targeted out-planting of coral at scale. Restor. Ecol. **28**: 886. doi:10.1111/rec.13070

Suslichenko, I. S., and A. N. Tikhonov. 2019. Photo-reducible plastoquinone pools in chloroplasts of *Tradescentia* plants acclimated to high and low light. FEBS Lett. **593**: 788–798. doi:10.1002/1873-3468.13366

Szabó, M., D. Wangpraseurt, B. Tamburic, A. W. D. Larkum, U. Schreiber, D. J. Suggett, M. Kühl, and P. J. Ralph. 2014. Effective light absorption and absolute electron transport rates in the coral *Pocillopora damicornis*. Plant Physiol. Biochem. **83**: 159–167. doi:10.1016/j.plaphy.2014.07.015

Szabó, M., and others. 2017. Non-intrusive assessment of photosystem II and photosystem I in whole coral tissues. Front. Mar. Sci. **4**: 269. doi:10.3389/fmars.2017.00269

Ulstrup, K. E., M. J. H. Van Oppen, M. Kühl, and P. J. Ralph. 2007. Inter-polyp genetic and physiological characterisation of *Symbiodinium* in an *Acropora valida* colony. Mar. Biol. **153**: 225–234. doi:10.1007/s00227-007-0806-x

Vega de Luna, F., J. J. Córdoba-Granados, K. Van Dang, S. Roberty, and P. Cardol. 2020. In vivo assessment of mitochondrial respiratory alternative oxidase activity and cyclic

electron flow around photosystem I on small coral fragments. Sci. Rep. **10**: 1–13. doi:10.1038/s41598-020-74557-0

Wangpraseurt, D., B. Tamburic, M. N. Szabó, D. Suggett, P. J. Ralph, and M. Kühl. 2014. Spectral effects on *Symbiodinium* photobiology studied with a programmable light engine. PLoS One **9**: e112809. doi:10.1371/journal.pone.0112809

Wangpraseurt, D., M. Lichtenberg, S. L. Jacques, A. W. D. Larkum, and M. Kühl. 2019. Optical properties of corals distort variable chlorophyll fluorescence measurements. Plant Physiol. **179**: 1608–1619. doi:10.1104/pp.18.01275

Warner, M. E., W. K. Fitt, and G. W. Schmidt. 1999. Damage to photosystem II in symbiotic dinoflagellates: A determinant of coral bleaching. Proc. Natl. Acad. Sci. USA **96**: 8007–8012. doi:10.1073/pnas.96.14.8007

Warner, M. E., T. C. LaJeunesse, J. D. Robison, and R. M. Thur. 2006. The ecological distribution and comparative photobiology of symbiotic dinoflagellates from reef corals in Belize: Potential implications for coral bleaching. Limnol. Oceanogr. **51**: 1887–1897. doi:10.4319/lo.2006.51.4.1887

Warner, M. E., M. P. Lesser, and P. J. Ralph. 2010. Chlorophyll fluorescence in reef building corals, p. 209–222. *In* Chlorophyll *a* fluorescence in aquatic sciences: Methods and applications. Springer.

Warner, M. E., and D. J. Suggett. 2016. The photobiology of *Symbiodinium* spp.: Linking physiological diversity to the implications of stress and resilience, p. 489–509. *In* The Cnidaria, past, present and future. Springer International Publishing.

Wickham, H. 2016. ggplot2: Elegant graphics for data analysis. Second Edition. Springer, p.260. doi:10.1007/978-3-319-24277-4

Wong, J. C. Y., S. Enríquez, and D. M. Baker. 2021. Towards a trait-based understanding of Symbiodiniaceae nutrient acquisition strategies. Coral Reefs **40**: 625–639. doi:10.1007/s00338-020-02034-1

Yang, W., H. Feng, X. Zhang, J. Zhang, J. H. Doonan, W. D. Batchelor, L. Xiong, and J. Yan. 2020. Crop phenomics and high-throughput phenotyping: Past decades, current challenges, and future perspectives. Mol. Plant **13**: 187–214. doi:10.1016/j.molp.2020.01.008

Yao, J., D. Sun, H. Cen, H. Xu, H. Weng, F. Yuan, and Y. He. 2018. Phenotyping of *Arabidopsis* drought stress response using kinetic chlorophyll fluorescence and multicolor fluorescence imaging. Front. Plant Sci. **9**: 603. doi:10.3389/fpls.2018.00603

Ziegler, M., C. M. Roder, C. Büchel, and C. R. Voolstra. 2014. Limits to physiological plasticity of the coral *Pocillopora verrucosa* from the Central Red Sea. Coral Reefs **33**: 1115–1129. doi:10.1007/s00338-014-1192-8

Acknowledgments

We wish to express immense thanks to UTS personnel (Paul Brooks and Lucia Bennar) for technical support with all laboratory data collection and who, along with the *Future Reefs* research staff and students, have continuously supported maintenance of the Symbiodiniaceae culture collection and coral aquaria used here. Also, to the staff of *Wavelength Reef Cruises* (Port Douglas, QLD) for logistical support with field data collection and diving operations. All field-based sampling was conducted under Great Barrier Reef Marine Park Authority (GBMPRA) permits for Opal Reef (G18/40023.1 and G19/42553 to E.F., D.J.S. and J.E.). D.S. and D.H. extend particular thanks to Zbigniew Kolber for his tireless support with the LIFT-FRRf and sound-boarding the phenotyping concept (ASLO Ocean Sciences Meeting San Diego, February 2020). Vessel operations for this work were supported by funding from the Australian & Queensland Governments ("Solving the bottleneck of reef rehabilitation through boosting coral abundance: Miniaturising and mechanising coral out planting" to D.J.S., E.F.C., J.E.) and ARC Discovery Early Career Research Award (DE190100142) to E.F.C. Contribution of E.F.C. and A.G. was through the University of Technology Sydney Chancellor's Postdoctoral Research Fellowship and DE190100142. M.R.N. was supported by a Rutherford Foundation Postdoctoral Fellowship (Royal Society of New Zealand). Additional funding support for D.J.S. and D.H. in data collection and manuscript writing was provided through from an Australian Research Council (ARC) Discovery Project (DP180100074) to D.J.S.

Conflict of Interest

None declared.

Submitted 02 August 2021
Revised 23 December 2021
Accepted 06 January 2022

Associate editor: Tammi Richardson